Identification of REM Sleep Behavior Disorder by Magnetic Resonance Imaging and Machine Learning

Jie Mei, PhD[1*†], Shady Rahayel, PhD[2,3*], Christian Desrosiers, PhD[4], Ronald B. Postuma, MD[2,5], Jacques Montplaisir, MD, PhD, CRCPc[2,6], Julie Carrier, PhD[2,7,8], Oury Monchi, PhD[8,9], Johannes Frasnelli, MD[1,2#], Jean-François Gagnon, PhD[2,10#]

[1]Department of Anatomy, Université du Québec à Trois-Rivières, Trois-Rivières, QC, Canada
[2]Centre for Advanced Research in Sleep Medicine, Hôpital du Sacré-Coeur de Montréal, Montreal, QC, Canada
[3]Montreal Neurological Institute and Hospital, McGill University, Montreal, QC, Canada
[4]Department of Software and IT Engineering, École de technologie supérieure Montréal, Montreal, QC, Canada
[5]Department of Neurology, Montreal General Hospital, Montreal, QC, Canada
[6]Department of Psychiatry, Université de Montréal, Montreal, QC, Canada
[7]Department of Psychology, Université de Montréal, Montreal, QC, Canada
[8]Research Centre, Institut universitaire de gériatrie de Montréal, Montreal, QC, Canada
[9]Departments of Clinical Neurosciences, Radiology, and Hotchkiss Brain Institute, University of Calgary, Calgary, Alberta, Canada
[10]Department of Psychology, Université du Québec à Montréal, Montreal, QC, Canada

*These authors contributed equally to this work.
[#]These authors share senior authorship.
[†]Current affiliation: 1. The Brain and Mind Institute, University of Western Ontario, London, ON, Canada. 2. Department of Computer Science, University of Western Ontario, London, ON, Canada

Contact information:
Dr. Jean-François Gagnon, Département de psychologie, Université du Québec à Montréal
C.P. 8888 succ. Centre-ville, Montréal (Québec), H3C 3P8, Canada
Email: gagnon.jean-francois.2@uqam.ca

Word count: 3698

Running title: Identification of RBD using machine learning

Conflict of interest: The authors declare that there is no conflict of interest.

Funding sources: The Canadian Institutes of Health Research (CIHR), the Fonds de recherche du Québec – Santé (FRQ-S), the Réseau intersectoriel de recherche en santé de l'Université du Québec (RISUQ), the Centre de recherche en neurosciences cognitives de l'Université du Québec à Montréal (NeuroQAM), Parkinson Canada, and the W. Garfield Weston Foundation.

Abstract

Background

Idiopathic rapid eye movement sleep behavior disorder (iRBD) is a major risk factor for synucleinopathies, and patients often present with clinical signs and morphological brain changes. However, there is a heterogeneity in the presentation and progression of these alterations, and brain regions that are more vulnerable to neurodegeneration remain to be determined.

Objectives

To assess the feasibility of morphology-based machine learning in the identification and subtyping of iRBD.

Methods

For the classification tasks [iRBD (n=48) vs controls (n=41); iRBD vs Parkinson's disease (n=29); iRBD with mild cognitive impairment (n=16) vs without mild cognitive impairment (n=32)], machine learning models were trained with morphometric measurements (thickness, surface area, volume, and deformation) extracted from T1-weighted structural magnetic resonance imaging. Model performance and the most discriminative brain regions were analyzed and identified.

Results

A high accuracy was reported for iRBD vs controls (79.6%, deformation of the caudal middle frontal gyrus and putamen, thinning of the superior frontal gyrus, and reduced volume of the inferior parietal cortex and insula), iRBD vs Parkinson's disease (82%, smaller volume and surface area of the insula, lower thinning of the entorhinal cortex and lingual gyrus, and greater volume of the fusiform gyrus), and iRBD with vs without mild cognitive impairment (84.8%, thinning of the pars triangularis, superior temporal gyrus, transverse temporal cortex, larger surface area of the superior temporal gyrus, and deformation of isthmus of the cingulate gyrus).

Conclusions

Morphology-based machine learning approaches may allow for detection and subtyping of iRBD, potentially enabling efficient preclinical identification of synucleinopathies.

Introduction

Isolated/idiopathic rapid eye movement (REM) sleep behavior disorder (iRBD) is a parasomnia characterized by loss of muscle atonia and abnormal motor manifestations during REM sleep (1). iRBD is a prodromal alpha-synucleinopathy, with most patients developing Parkinson's disease (PD) or dementia with Lewy bodies (DLB) over time (2). iRBD patients already show clinical and brain changes that are reminiscent of overt synucleinopathies (3–5), including cognitive impairment and brain atrophy (1,4-7). However, the identification and progression of these changes vary widely in the iRBD population (4-7). In particular, mild cognitive impairment (MCI), present in about one third of iRBD patients (5,6), is associated with a higher likelihood of phenoconversion to a dementia- compared to a parkinsonism-first phenotype (5,6,8).

Studies using structural magnetic resonance imaging (MRI) in iRBD reported extensive cortical and subcortical changes (4,5,7,9–14), which are more pronounced in patients with MCI (5,15). Findings have included frontal, temporal and occipital cortical thinning (9–11), subcortical shape contraction in the basal ganglia and hippocampus (10,12), and gray matter volume alterations in the prefrontal cortex, caudate, brainstem, cerebellum, and parahippocampal gyrus (9,13,14). Moreover, a brain volume deformation signature that could predict development of DLB at the individual level has been identified in iRBD (16). However, most of these studies have only looked at morphological changes one metric at a time, thereby preventing identifying sets of regions that may discriminate between iRBD patients and healthy individuals (controls) or between iRBD subtypes (presence of MCI), while taking into consideration several different morphological features that can be derived from every brain region.

Machine learning have been increasingly applied to the identification and prognosis of neurodegenerative diseases including PD and DLB (17–20). Few studies have used machine learning for the identification of iRBD with polysomnogram (PSG), electroencephalogram (EEG), motor, and olfaction measures (21–25). To our knowledge, only one study has applied machine learning to diffusion tensor imaging for the identification of iRBD vs controls, and achieved an accuracy of 87.5% (26). However, this study has a small sample size and no distinction based on the cognitive profile. Given the ability of brain changes, mainly those associated with gray matter alterations, to identify MCI and predict phenoconversion in iRBD (15,16), an assessment of morphometric changes, along with a thorough evaluation of the discriminative power of single versus multiple brain region(s) in the identification and subtyping of iRBD, is of relevance. Moreover, machine learning has been applied to the extraction of relevant pre-clinical and clinical features, and can be used in inter-modality registration of different types of data (17,27), potentially enabling improved identification of iRBD.

In this study, we derived regional brain morphological measurements including cortical thickness, volume, surface area and tissue deformation to assess whether machine learning models differentiate between **(a)** iRBD patients and controls, **(b)** iRBD and PD patients, and **(c)** iRBD patients with and without MCI. We hypothesized brain morphology can differentiate between controls, PD patients and iRBD subtypes with high accuracy.

Methods

Participants

iRBD patients were enrolled at the Centre for Advanced Research in Sleep Medicine of the *Centre Intégré universitaire de santé et de services sociaux du Nord-de-l'Île-de-Montréal – Hôpital du Sacré-Cœur de Montréal (CIUSS-NÎM-HSCM)*. All patients met the diagnostic criteria for iRBD based on the International Classification of Sleep Disorders, Third Edition and PSG (28,29). iRBD patients were excluded if they presented with parkinsonism or dementia (30,31). A history of brain injury, head trauma, stroke, claustrophobia, EEG abnormalities suggesting epilepsy, encephalitis, or other neurological disorders also led to exclusion. Controls without PD, iRBD, and MCI were recruited through newspaper advertisements or by word of mouth. They were subjected to the same exclusion criteria as iRBD patients. All participants were part of previous studies on neuroimaging in iRBD (9,12,15,16,32).

PD patients were recruited from the Department of Neurology of the Montreal General Hospital and the *Unité des troubles du mouvement André-Barbeau* of the *Centre Hospitalier de l'Université de Montréal*. Inclusion criteria were: 1) a diagnosis of idiopathic PD as the likeliest cause (30), 2) being 45-85 years old, 3) disease duration ≤10 years, 4) Hoehn & Yahr stage ≤3, 5) absence of dementia or any major psychiatric disorder, 6) respiratory event index ≤20, and 7) absence of a history of head injury, stroke, brain tumor, cerebrovascular disease, and chronic obstructive pulmonary disease or abnormal EEG features suggesting epilepsy. These patients were part of previous studies on neuroimaging in PD (16,33).

All participants were part of research protocols approved by local ethics committees (CIUSSS-NÎM-HSCM) and CIUSSS *du Centre-Sud-de-l'Île-de-Montréal – Comité d'éthique de la recherche vieillissement-neuroimagerie,* Montreal, Canada) and provided written informed consent.

Neuropsychological assessment

Participants underwent neurological and neuropsychological assessments including the Unified Parkinson's Disease Rating Scale part III (34), and, in iRBD patients only, the Montreal Cognitive assessment (MoCA) for cognitive screening (35). MCI was diagnosed with the neuropsychological assessment and a consensus between the neurologist and neuropsychologist based on the following criteria: 1) subjective cognitive complaints by the patient, the spouse or the caregiver, as measured using the Cognitive Failures Questionnaire (36) or as assessed during the semi-structured interview, 2) the presence of objective cognitive impairment, as defined by a performance score at least 1.5 SD

below the standardized mean on at least 2 tasks within a single cognitive domain, namely attention/executive functions, learning and verbal memory, or visuospatial abilities, 3) preserved daily life functioning, 4) no dementia, and 5) cognitive deficits not being explained solely by a medication or another medical condition (8,15).

MRI

Acquisition

T1-weighted scans were acquired in all participants using a 3T Siemens TrioTIM scanner with a 12-channel head matrix coil and an MP-RAGE sequence (parameters: repetition time: 2.3s, echo time: 2.91ms, inversion time: 900ms, flip angle: 9°, field of view: 256×240mm, matrix resolution: 256×240mm, voxel size: 1×1×1mm, bandwidth: 240Hz/Px, 160 slices).

Morphological processing

Cortical surface processing was first conducted using FreeSurfer, version 6.0.0 (37,38). Processing steps included non-brain tissue removal, Talairach transformation, segmentation of subcortical white matter and gray matter subcortical volumetric structures, intensity normalization, and cortical reconstruction. Quality control was performed visually at a slice level and pial and white matter surface errors were corrected manually by a trained rater (S.R.). Cortical thickness, surface area, and volume maps were then parcellated into 34 cortical regions per hemisphere using the Desikan-Killiany atlas (39). Regional surface area and volume values were normalized by the estimated total intracranial volume since these measurements scale with head size.

Deformation-based morphometry (DBM) processing was applied to the T1-weighted images using CAT12 (http://www.neuro.uni-jena.de/cat/) to generate gray matter tissue deformation maps. DBM quantified volume differences by computing the deformations needed to perform nonlinear transformation of an individual brain to a template space (40). The Jacobian determinant maps were smoothed using a 12-mm FWHM kernel and used as a marker of local brain deformation. Maps were parcellated into 83 regions, namely 34 cortical and 7 subcortical regions (putamen, caudate, pallidum, thalamus, hippocampus, amygdala, accumbens area) for each hemisphere plus the brainstem, according to the Desikan-Killiany atlas (39). The deformation value of each region represented the mean deformation of all voxels assigned to the region.

Feature selection and machine learning

We first performed feature selection to identify morphometric measurements with high discriminative power. To ensure no data were used both for feature selection and model validation, the dataset was split into a training set and a test set in a stratified manner. To understand whether feature selection and model performance were affected by patient distribution of the train-test split, splitting was performed for 25 times using a train:test split ratio of 9:1 (for iRBD vs controls and iRBD vs PD) or 4:1 (for iRBD with MCI vs iRBD without MCI), to generate 25 unique splits for obtaining the averaged model performance (Supplementary Figure 1). Given the number of features (68, 68, 68, and 83 for thickness, surface area, volume and deformation respectively), we used a random forest classifier (n_estimators = 10) on the training set with 5-fold cross-validation to select features based on relative importance averaged over 1,000 iterations.

For the discrimination between iRBD and control, machine learning models were trained with 1, 2, 3, or 5 out of the 15-20 most relevant brain regions for each individual modality. To examine whether combining different morphometric modalities leads to higher model performance, we performed the same procedures after combining regional measurements across modalities (n=287). For iRBD vs PD patients and iRBD patients with MCI vs without MCI, we merged across all modalities for model training without examining classification performance of individual modalities.

We used an expanded grid-search with 5-fold cross-validation to search through models including: 1) logistic regression, 2) decision tree, 3) random forest, 4) k-nearest neighbors (KNN), 5) support vector machine (SVM), and 6) boosting models, and their hyperparameters. All morphometric measurements were centered to the mean and scaled to unit variance. All procedures were implemented using Scikit-learn, version 0.17 (41).

Model evaluation and statistical analysis

To identify brain regions showing atrophy, we performed Mann-Whitney U tests followed by the Benjamini-Hochberg procedure for controlling false discovery for multiple comparisons (42). Given the imbalanced dataset, in addition to accuracy, metrics including recall, precision, and F1-score were used. Recall, also known as sensitivity or true positive rate, is defined as the number of true positives divided by the sum of true positives and false negatives. Precision is defined as the number of true positives divided by the sum of true positives and false positives. The F1-score is the harmonic mean of precision and recall, and accuracy indicates the ratio of number of correct predictions to number of all predictions. Data are shown as mean (SD). Statistical analyses were performed using pandas, version 0.25.3 (43) and scikit-posthocs, version 0.6.7 (44).

Results

Demographics and clinical data

Of the 59 iRBD patients recruited, 11 were excluded for parkinsonism or dementia at presentation or unclear clinical presentation/borderline electromyogram thresholds for REM sleep muscle atonia. All participants survived quality control except for one PD patient who had abnormal surface reconstruction in the occipital lobe, yielding 48 iRBD patients, 29 PD patients [mean (SD), PD duration since diagnosis: 3.8 (2.7) years; levodopa equivalent dosage: 536.5 (283.1) mg/daily; Hoehn & Yahr stage: 2.2 (0.8); 41% (12/29) with MCI; 48% (14/29) with RBD], and 41 controls (Table 1) for MRI processing. Sixteen (33%) iRBD patients had MCI. There were no significant differences in age and education between the groups. The proportion of men was higher in iRBD than PD patients. PD had a higher UPDRS-III total score than iRBD patients. Moreover, iRBD patients with MCI performed poorer than those without MCI on the MoCA.

Insert Table 1 here

Morphometric measurements

Of the 287 morphometric features, 37 (12.9%) significantly differed between iRBD patients and controls, 20 (7.0%) between iRBD and PD patients, and 27 (9.4%) between iRBD patients with or without MCI (Supplementary Tables 1, 4 and 5). Compared to controls, iRBD patients had cortical thinning, reduced volume, and tissue deformation in several brain regions (Supplementary Table 1). Compared to PD, iRBD patients had mixed results for cortical thickness, but with reduced volume in PD (bilateral fusiform gyrus) and tissue deformation, mainly in left subcortical regions, in iRBD (Supplementary Table 4). Compared to patients without MCI, those with MCI had cortical thinning, larger surface area, and tissue deformation, mainly in posterior regions (Supplementary Table 5).

Feature importance and machine learning-based classification

Although 5 brain regions that contributed to the highest overall model performance were reported, it should be noted that in all classification tasks, feature importance of the most

relevant brain regions (top 5%-10%) were often comparable (Supplementary Tables 2 and 3) and could lead to classification performance that was only 2%-5% lower than the reported results.

iRBD vs Controls

The highest accuracy (79.6%) was obtained when measurements of all morphometric modalities were merged to select 5 features for model training, namely deformation of the left caudal middle frontal gyrus and right putamen, thinning of the left superior frontal gyrus, and reduced volume of the right inferior parietal cortex and insula (Table 2 and Figures 1a-e and 2). When using single modalities for model training, a classification accuracy of 79.1% was achieved with 5 features selected from DBM-based measurements, namely tissue deformation in the left caudal middle frontal gyrus, paracentral lobule, thalamus, and bilateral putamen. When training the model with 1 feature derived from DBM or across all modalities, deformation of the left caudal middle frontal gyrus led to an accuracy of 71.1%.

Depending on the modality used, linear SVM or SVM with a radial basis function (RBF) was the best performing model in most, if not all, of the 25 randomly generated train-test splits (Table 2; n=24.95 (0.22); range=24-25). As indicated by the relative importance, cortical regions, including the left caudal middle frontal cortex (reduced volume, deformation), paracentral lobule (reduced volume, deformation), and superior frontal cortex (thinning), as well as the right inferior parietal cortex (reduced volume), and insula (reduced volume), yielded high discriminative power for the detection of iRBD (Table 2; Supplementary Tables 2 and 3).

_____

Insert Table 2 here

_____

_____

Insert Figure 1 here

_____

_____

Insert Figure 2 here

_____

iRBD vs PD

With morphometric measurements of 5 brain regions, including, in iRBD, a smaller volume and surface area of the right insula, lower thinning of the right entorhinal cortex and lingual gyrus, and greater volume of the right fusiform gyrus, an accuracy of 82% was achieved (Table 2; Figures 1f and 2). When morphometric measurements of single brain regions were used to train the machine learning model, smaller volume of the right insula in iRBD led to an accuracy of 70% (Table 2). SVM with an RBF kernel demonstrated the highest performance in a majority of the 25 randomly generated train-test splits (n=24.75 (0.5); range=24-25).

iRBD with MCI vs iRBD without MCI

An accuracy of 84.8% was obtained from a model trained with all morphometric measurements of 5 brain regions, namely thinning of the left transverse temporal cortex, pars triangularis and superior temporal gyrus, larger surface area of the left superior temporal gyrus, and deformation of isthmus of the right cingulate gyrus in iRBD patients with MCI (Table 2; Figures 1g and 2). When using single brain regions (thinning of the left pars triangularis in iRBD with MCI) or 2 regions (thinning of the left pars triangularis and superior temporal gyrus in iRBD with MCI), a decision tree classifier of depth 1 achieved an accuracy of 72.8% and 73.2%, respectively (Table 2; Figures 1g and 2). When more brain regions were used, a linear SVM yielded the highest overall performance in most of the train-test splits (n=22.5 (0.71); range=22-23).

Discussion

General observations

In this study, we derived a comprehensive set of morphological regional brain measurements and used machine learning to identify regions that best discriminate between iRBD patients and controls, iRBD and PD patients, and cognitive subtypes of iRBD. We showed that machine learning models trained with morphometric measurements efficiently differentiate between iRBD and controls (accuracy=79.6%), iRBD and PD (accuracy=82%), and iRBD with or without MCI (accuracy=84.8%) and may prove useful for guiding future algorithms that discriminate patients based on structural MRI.

When discriminating iRBD patients from controls with all morphometric modalities, an accuracy of 79.6% was achieved by models trained using deformation of the left caudal middle frontal gyrus and right putamen, thinning of the left superior frontal gyrus, and reduced volume of the right inferior parietal cortex and insula. With single modalities, an accuracy of 79.1% was obtained from models trained with DBM-derived data, i.e., tissue deformation in the left caudal middle frontal gyrus, paracentral lobule, thalamus, and bilateral putamen. For the other modalities, namely cortical surface-derived measures of thickness, surface area or volume, a lower but above-chance-level accuracy was also observed. This supports the importance of tissue deformation in the structural pattern of atrophy seen in iRBD, as well as the importance of taking into consideration the changes occurring in subcortical regions in iRBD (6,9,10,12-14). The model trained with greater volume and surface area of the right insula, thinning of the right entorhinal cortex and lingual gyrus, and reduced volume of the right fusiform gyrus led to an accuracy of 82% in the discrimination of iRBD from PD patients. Furthermore, an accuracy of 84.8% was obtained in the identification of iRBD patients with MCI, from a model trained with thinning of the left transverse temporal cortex, pars triangularis and superior temporal gyrus, larger surface area of the left superior temporal gyrus, and deformation of isthmus of the right cingulate gyrus.

Few studies have used machine learning to identify iRBD patients with MRI, EEG/PSG, or clinical markers. One study used machine learning models with diffusion tensor imaging measures and found structural differences between 20 iRBD patients and 20 controls, enabling identification of iRBD with an accuracy of 87.5% (26). One study derived features from EEG signals during sleep to train a random forest model that identified iRBD vs controls with an accuracy of 96%, a sensitivity of 98%, and a specificity of 94% (24). In another study that used PSG data, electrooculogram signals were acquired for deriving features relevant to micro-sleep structure, which gave rise to

identification of iRBD patients in PD patients through micro-sleep instability, with accuracy, sensitivity, and specificity over 80% (22). In a longitudinal study (23), resting EEG data were analyzed using a convolutional neural network and a recurrent neural network. The two achieved comparable results, leading to an accuracy of 80% when predicting conversion to PD in iRBD. One study used sensor data recorded during motor tasks and trained random forest classifiers to distinguish controls, iRBD and PD patients, and obtained a sensitivity ranging from 84.6% to 91.9%, and a specificity ranging from 88.3% to 90.1% (25). Another study used olfaction data (21) and reported an area under the curve value of ≥0.90 when classifying between iRBD and PD. While these studies demonstrated a high accuracy in the identification of iRBD or PD, many are based on motor features that appear at a later stage of neurodegeneration as in patients at risk of DLB. Moreover, in motor tasks and EEG/PSG, data acquisition can take up to days, making quality control and follow-ups challenging. In addition, previous studies have not attempted to subtype between iRBD patients with or without MCI, for which we have achieved an accuracy of 84.8%. This is essential given the large heterogeneity of cognitive impairment reported in iRBD patients, and the higher risk of developing DLB or PD with cognitive impairment in iRBD patients with MCI. Comparing with these studies, the present study also highlights structural brain changes that allow the identification and subtyping of iRBD.

Deformation of putamen and thalamus, and thinning of caudal middle frontal and paracentral cortices best distinguished between iRBD patients and controls. This is in line with studies performed on the same cohorts using single morphometric measures (12,15,16). Putamen dopamine depletion underlies parkinsonism (45), while the putamen is structurally and functionally abnormal in iRBD (12,46–50), as observed by reduced dopamine reuptake imaging (5,47) and perfusion/metabolism imaging (48–50). The smaller volume of the insula in iRBD was also found to discriminate between iRBD and PD. In the present study, greater thinning of the left insula was observed in iRBD patients with MCI, and the presence of MCI in iRBD is a risk factor for DLB (5,6,8), which is in agreement with studies reporting the insula as highly associated with prodromal and clinical DLB (51–54). Its ability to discriminate between iRBD and PD may therefore be due to some iRBD patients being on a dementia-first trajectory. Also, in accordance with studies that used morphometric measures of the fusiform gyrus to detect PD (55,56), our study highlighted the volume of the fusiform gyrus as a discriminative feature.

Compared to surface-derived cortical metrics assessing local thickness, surface area or volume, DBM-derived tissue deformation measurements generated higher discriminative power between iRBD patients and controls. This is important, as different morphological metrics were shown to follow different developmental trajectories (57), to relate to different genetic determinants (58,59), and to be affected differentially in neurodegenerative prodromes (15,60). Several reasons can explain the fact that DBM is

most discriminative. First, DBM maps included information about subcortical structures, which are known to be affected in iRBD (9,10). Secondly, white matter changes are an increasingly recognized feature of neurodegeneration in PD and DLB (61,62); although tissue deformation measurements were extracted from the gray matter only, it is possible that gray matter deformation may have been influenced by dynamics occurring in the underlying white matter. This is even more important as some studies have reported white matter abnormalities in iRBD (14,63,64). Recently, we identified in the same cohort of iRBD patients a DBM-derived structural signature that predicts the development of DLB in iRBD; interestingly, white matter tissue contraction was an important feature of this signature (16). Future studies should investigate the association between changes in gray and white matter in iRBD.

We also found that some of the discriminative brain regions in the classification between iRBD patients and controls, and the identification of PD patients (e.g., the medial orbitofrontal cortex and pars orbitalis) are involved in olfactory processing. Morphometric measures of olfactory processing areas in the orbitofrontal cortex such as the olfactory sulcus, the gyrus rectus, and the medial orbitofrontal cortex are associated with olfactory sensitivity (65,66). Further, olfactory function is impaired in both PD and iRBD patients (3,67). We have shown in a previous study that a convolutional neural network can distinguish PD patients from patients with non-parkinsonian olfactory dysfunction (68). In the future, olfaction and other markers of motor or cognitive performance could be combined with morphometric measures to increase the specificity and sensitivity of iRBD identification (5).

Limitations

From a clinical perspective, brain imaging data used in this study were collected from a considerable number of participants. However, they represent a relatively small sample size when compared with deep learning studies using multicentric data, or with studies applying machine learning and deep learning to iRBD detection using PSG or EEG features. To enable computer-aided decision-making in the identification and subtyping of iRBD, studies using a larger prospective-longitudinal cohort are required. In addition, it has been shown that the version of the preprocessing pipeline may become a confounding factor in the assessment of neurological disorders (69), therefore, it would be crucial to understand to what extent the detection of iRBD is affected by the preprocessing pipeline, and/or the software version used.

Author roles

J. Mei: Conception and execution of research project, design and execution of statistical analysis, writing the first draft of manuscript.
SR: Conception of research project, design, review and critique of statistical analysis, writing the first draft of manuscript.
CD: Review and critique of statistical analysis, review of manuscript.
RBP: Funding, organization of research project, data collection, review of manuscript.
J. Montplaisir: Funding, organization of research project, data collection, review of manuscript.
JC: Organization of research project, data collection, review of manuscript.
OM: Organization of research project, data collection, review of manuscript.
JF: Funding, organization and supervision of research project, review of manuscript.
JFG: Funding, organization and supervision of research project, data collection, writing and review of manuscript.

Acknowledgements

We would like to thank Amélie Pelletier and Jessie De Roy for their assistance in organizing data, and Sylvain Chouinard and Michel Panisset for clinical evaluations of PD patients. Shady Rahayel receives a scholarship from the Fonds de recherche du Québec – Santé. JFG holds a Canada Research Chair in Cognitive Decline in Pathological Aging.

Financial Disclosures

This work was supported by the Canadian Institutes of Health Research (CIHR), the *Fonds de recherche du Québec – Santé* (FRQ-S), the *Réseau intersectoriel de recherche en santé de l'Université du Québec* (RISUQ), the Centre de recherche en neurosciences cognitives de l'Université du Québec à Montréal (NeuroQAM), and the W. Garfield Weston Foundation. JFG received research grant outside this work from the National Institutes of Health/National Institute for Aging. This work was supported by grants from the Canadian Institutes of Health Research (CIHR, PJT173514) and Parkinson Canada (PPG-2020-0000000061) to JF.

J. Mei:
Stock Ownership in medically-related fields: Oyama Health AB
Consultancies: deepkapha.ai, Oyama Health AB
Employment: Université du Québec à Trois-Rivières, University of Western Ontario
Grants: BrainsCAN Postdoctoral Fellowship Award through Canada First Research Excellence Fund (CFREF)

Partnerships: Charité Global Health

JF:
Employment: Université du Québec à Trois-Rivières
Royalties: Styriabooks
Grants: FRQS, NSERC, CIHR

References

1. Högl B, Stefani A, Videnovic A. Idiopathic REM sleep behaviour disorder and neurodegeneration - an update. Nat Rev Neurol. 2018 Jan;14(1):40–55.

2. Postuma RB, Iranzo A, Hu M, Högl B, Boeve BF, Manni R, et al. Risk and predictors of dementia and parkinsonism in idiopathic REM sleep behaviour disorder: a multicentre study. Brain. 2019 Mar 1;142(3):744–59.

3. Fereshtehnejad S-M, Yao C, Pelletier A, Montplaisir JY, Gagnon J-F, Postuma RB. Evolution of prodromal Parkinson's disease and dementia with Lewy bodies: a prospective study. Brain. 2019 Jul 1;142(7):2051–67.

4. Bourgouin P-A, Rahayel S, Gaubert M, Arnaldi D, Hu M, Heidbreder A, et al. Neuroimaging of Rapid Eye Movement Sleep Behavior Disorder. Int Rev Neurobiol. 2019;144:185–210.

5. Miglis MG, Adler CH, Antelmi E, Arnaldi D, Baldelli L, Boeve BF, et al. Biomarkers of conversion to α-synucleinopathy in isolated rapid-eye-movement sleep behaviour disorder. The Lancet Neurology. 2021 Aug 1;20(8):671–84.

6. Gagnon J, Bourgouin P, Roy J, Marchand DG. Neuropsychological Aspects: Cognition in RBD. In 2019.

7. Campabadal A, Segura B, Junque C, Iranzo A. Structural and functional magnetic resonance imaging in isolated REM sleep behavior disorder: A systematic review of studies using neuroimaging software. Sleep Med Rev. 2021 Apr 22;59:101495.

8. Génier Marchand D, Montplaisir J, Postuma RB, Rahayel S, Gagnon J-F. Detecting the Cognitive Prodrome of Dementia with Lewy Bodies: A Prospective Study of REM Sleep Behavior Disorder. Sleep. 2017 Jan 1;40(1).

9. Rahayel S, Montplaisir J, Monchi O, Bedetti C, Postuma RB, Brambati S, et al. Patterns of cortical thinning in idiopathic rapid eye movement sleep behavior disorder. Mov Disord. 2015 Apr 15;30(5):680–7.

10. Campabadal A, Segura B, Junque C, Serradell M, Abos A, Uribe C, et al. Cortical Gray Matter and Hippocampal Atrophy in Idiopathic Rapid Eye Movement Sleep Behavior Disorder. Front Neurol. 2019 Apr 5;10:312.

11. Pereira JB, Weintraub D, Chahine L, Aarsland D, Hansson O, Westman E. Cortical thinning in patients with REM sleep behavior disorder is associated with clinical progression. NPJ Parkinsons Dis. 2019 May 3;5:7.

12. Rahayel S, Postuma RB, Montplaisir J, Bedetti C, Brambati S, Carrier J, et al. Abnormal Gray Matter Shape, Thickness, and Volume in the Motor Cortico-Subcortical Loop in Idiopathic Rapid Eye Movement Sleep Behavior Disorder: Association with Clinical and Motor Features. Cereb Cortex. 2018 Feb 1;28(2):658–71.

13. Hanyu H, Inoue Y, Sakurai H, Kanetaka H, Nakamura M, Miyamoto T, et al. Voxel-based magnetic resonance imaging study of structural brain changes in patients with idiopathic REM sleep behavior disorder. Parkinsonism Relat Disord. 2012 Feb;18(2):136–9.

14. Holtbernd F, Romanzetti S, Oertel WH, Knake S, Sittig E, Heidbreder A, et al. Convergent patterns of structural brain changes in rapid eye movement sleep behavior disorder and Parkinson's disease on behalf of the German rapid eye movement sleep behavior disorder study group. Sleep. 2021 Mar 12;44(3):zsaa199.

15. Rahayel S, Postuma RB, Montplaisir J, Génier Marchand D, Escudier F, Gaubert M, et al. Cortical and subcortical gray matter bases of cognitive deficits in REM sleep behavior disorder. Neurology. 2018 May 15;90(20):e1759–70.

16. Rahayel S, Postuma RB, Montplaisir J, Mišić B, Tremblay C, Vo A, et al. A Prodromal Brain-Clinical Pattern of Cognition in Synucleinopathies. Ann Neurol. 2021 Feb;89(2):341–57.

17. Mei J, Desrosiers C, Frasnelli J. Machine Learning for the Diagnosis of Parkinson's Disease: A Review of Literature. Front Aging Neurosci [Internet]. 2021 [cited 2021 Jul 19];0. Available from: https://www.frontiersin.org/articles/10.3389/fnagi.2021.633752/full

18. Iizuka T, Fukasawa M, Kameyama M. Deep-learning-based imaging-classification identified cingulate island sign in dementia with Lewy bodies. Sci Rep. 2019 Jun 20;9(1):8944.

19. Shigemizu D, Akiyama S, Asanomi Y, Boroevich KA, Sharma A, Tsunoda T, et al. A comparison of machine learning classifiers for dementia with Lewy bodies using miRNA expression data. BMC Medical Genomics. 2019 Oct 30;12(1):150.

20. Nemoto K, Sakaguchi H, Kasai W, Hotta M, Kamei R, Noguchi T, et al. Differentiating Dementia with Lewy Bodies and Alzheimer's Disease by Deep Learning to Structural MRI. Journal of Neuroimaging. 2021;31(3):579–87.

21. Lo C, Arora S, Ben-Shlomo Y, Barber TR, Lawton M, Klein JC, et al. Olfactory Testing in Parkinson Disease and REM Behavior Disorder: A Machine Learning Approach. Neurology. 2021 Apr 13;96(15):e2016–27.

22. Cesari M, Christensen JAE, Muntean M-L, Mollenhauer B, Sixel-Döring F, Sorensen HBD, et al. A data-driven system to identify REM sleep behavior disorder and to predict its progression from the prodromal stage in Parkinson's disease. Sleep Med. 2021 Jan;77:238–48.

23. Ruffini G, Ibañez D, Castellano M, Dubreuil-Vall L, Soria-Frisch A, Postuma R, et al. Deep Learning With EEG Spectrograms in Rapid Eye Movement Behavior Disorder. Front Neurol [Internet]. 2019 [cited 2021 Jul 19];0. Available from: https://www.frontiersin.org/articles/10.3389/fneur.2019.00806/full

24. Cooray N, Andreotti F, Lo C, Symmonds M, Hu MTM, De Vos M. Detection of REM sleep behaviour disorder by automated polysomnography analysis. Clin Neurophysiol. 2019 Apr;130(4):505–14.

25. Arora S, Baig F, Lo C, Barber TR, Lawton MA, Zhan A, et al. Smartphone motor testing to distinguish idiopathic REM sleep behavior disorder, controls, and PD. Neurology. 2018 Oct 16;91(16):e1528–38.

26. Lee DA, Lee H-J, Kim HC, Park KM. Application of machine learning analysis based on diffusion tensor imaging to identify REM sleep behavior disorder. Sleep Breath. 2021 Jul 8;

27. Huang S-C, Pareek A, Seyyedi S, Banerjee I, Lungren MP. Fusion of medical imaging and electronic health records using deep learning: a systematic review and implementation guidelines. npj Digit Med. 2020 Oct 16;3(1):1–9.

28. Montplaisir J, Gagnon J-F, Fantini ML, Postuma RB, Dauvilliers Y, Desautels A, et al. Polysomnographic diagnosis of idiopathic REM sleep behavior disorder. Mov Disord. 2010 Oct 15;25(13):2044–51.

29. American Academy of Sleep Medicine. International Classification of Sleep Disorders. Diagnostic and Coding Manual [Internet]. 2014 [cited 2021 Sep 17]; Available from: https://ci.nii.ac.jp/naid/20001061569/

30. Postuma RB, Berg D, Stern M, Poewe W, Olanow CW, Oertel W, et al. MDS clinical diagnostic criteria for Parkinson's disease. Mov Disord. 2015 Oct;30(12):1591–601.

31. McKeith IG, Boeve BF, Dickson DW, Halliday G, Taylor J-P, Weintraub D, et al. Diagnosis and management of dementia with Lewy bodies: Fourth consensus report of the DLB Consortium. Neurology. 2017 Jul 4;89(1):88–100.

32. Bourgouin P-A, Rahayel S, Gaubert M, Postuma RB, Montplaisir J, Carrier J, et al. Gray matter substrates of depressive and anxiety symptoms in idiopathic REM sleep behavior disorder. Parkinsonism Relat Disord. 2019 May;62:163–70.

33. Rahayel S, Gaubert M, Postuma RB, Montplaisir J, Carrier J, Monchi O, et al. Brain atrophy in Parkinson's disease with polysomnography-confirmed REM sleep behavior disorder. Sleep [Internet]. 2019 Jun 11 [cited 2021 Jul 19];42(6). Available from: https://doi.org/10.1093/sleep/zsz062

34. Fahn S, Elton R, Members of the UPDRS Development Committee. Recent developments in Parkinson's disease. Macmillan health care information. 1987;2, 153–163:293–304.

35. Nasreddine ZS, Phillips NA, Bédirian V, Charbonneau S, Whitehead V, Collin I, et al. The Montreal Cognitive Assessment, MoCA: a brief screening tool for mild cognitive impairment. J Am Geriatr Soc. 2005 Apr;53(4):695–9.

36. Broadbent DE, Cooper PF, FitzGerald P, Parkes KR. The Cognitive Failures Questionnaire (CFQ) and its correlates. Br J Clin Psychol. 1982 Feb;21(1):1–16.

37. Reuter M, Schmansky NJ, Rosas HD, Fischl B. Within-subject template estimation for unbiased longitudinal image analysis. Neuroimage. 2012 Jul 16;61(4):1402–18.

38. Dale AM, Fischl B, Sereno MI. Cortical surface-based analysis. I. Segmentation and surface reconstruction. Neuroimage. 1999 Feb;9(2):179–94.

39. Desikan RS, Ségonne F, Fischl B, Quinn BT, Dickerson BC, Blacker D, et al. An automated labeling system for subdividing the human cerebral cortex on MRI scans into gyral based regions of interest. NeuroImage. 2006 Jul 1;31(3):968–80.

40. Ashburner J, Hutton C, Frackowiak R, Johnsrude I, Price C, Friston K. Identifying global anatomical differences: deformation-based morphometry. Hum Brain Mapp. 1998;6(5–6):348–57.

41. Pedregosa F, Varoquaux G, Gramfort A, Michel V, Thirion B, Grisel O, et al. Scikit-learn: Machine Learning in Python. Journal of Machine Learning Research. 2011;12(Oct):2825–30.

42. Benjamini Y, Hochberg Y. Controlling the False Discovery Rate: A Practical and Powerful Approach to Multiple Testing. Journal of the Royal Statistical Society: Series B (Methodological). 1995;57(1):289–300.

43. McKinney W. Data Structures for Statistical Computing in Python. Proceedings of the 9th Python in Science Conference. 2010;56–61.

44. Terpilowski MA. scikit-posthocs: Pairwise multiple comparison tests in Python. Journal of Open Source Software. 2019 Apr 14;4(36):1169.

45. Politis M. Neuroimaging in Parkinson disease: from research setting to clinical practice. Nat Rev Neurol. 2014 Dec;10(12):708–22.

46. Rolinski M, Griffanti L, Piccini P, Roussakis AA, Szewczyk-Krolikowski K, Menke RA, et al. Basal ganglia dysfunction in idiopathic REM sleep behaviour disorder parallels that in early Parkinson's disease. Brain. 2016 Aug;139(8):2224–34.

47. Bauckneht M, Chincarini A, De Carli F, Terzaghi M, Morbelli S, Nobili F, et al. Presynaptic dopaminergic neuroimaging in REM sleep behavior disorder: A systematic review and meta-analysis. Sleep Med Rev. 2018 Oct;41:266–74.

48. Vendette M, Gagnon J-F, Soucy J-P, Gosselin N, Postuma RB, Tuineag M, et al. Brain perfusion and markers of neurodegeneration in rapid eye movement sleep behavior disorder. Mov Disord. 2011 Aug 1;26(9):1717–24.

49. Holtbernd F, Gagnon J-F, Postuma RB, Ma Y, Tang CC, Feigin A, et al. Abnormal metabolic network activity in REM sleep behavior disorder. Neurology. 2014 Feb 18;82(7):620–7.

50. Kim R, Lee J-Y, Kim YK, Kim H, Yoon EJ, Shin JH, et al. Longitudinal Changes in Isolated Rapid Eye Movement Sleep Behavior Disorder-Related Metabolic Pattern Expression. Mov Disord. 2021 Mar 31;

51. Zhong J, Pan P, Dai Z, Shi H. Voxelwise meta-analysis of gray matter abnormalities in dementia with Lewy bodies. Eur J Radiol. 2014 Oct;83(10):1870–4.

52. Blanc F, Colloby SJ, Philippi N, Pétigny X de, Jung B, Demuynck C, et al. Cortical Thickness in Dementia with Lewy Bodies and Alzheimer's Disease: A Comparison of Prodromal and Dementia Stages. PLOS ONE. 2015 Jun 10;10(6):e0127396.

53. Roquet D, Noblet V, Anthony P, Philippi N, Demuynck C, Cretin B, et al. Insular atrophy at the prodromal stage of dementia with Lewy bodies: a VBM DARTEL study. Sci Rep. 2017 Aug 25;7(1):9437.

54. Firbank MJ, Durcan R, O'Brien JT, Allan LM, Barker S, Ciafone J, et al. Hippocampal and insula volume in mild cognitive impairment with Lewy bodies. Parkinsonism & Related Disorders. 2021 May 1;86:27–33.

55. Peng B, Wang S, Zhou Z, Liu Y, Tong B, Zhang T, et al. A multilevel-ROI-features-based machine learning method for detection of morphometric biomarkers in Parkinson's disease. Neurosci Lett. 2017 Jun 9;651:88–94.

56. Mei J, Tremblay C, Stikov N, Desrosiers C, Frasnelli J. Differentiation of Parkinson's disease and non-Parkinsonian olfactory dysfunction with structural MRI data. In: Medical Imaging 2021: Computer-Aided Diagnosis [Internet]. International Society for Optics and Photonics; 2021 [cited 2021 Jul 19]. p. 115971E. Available from: https://www.spiedigitallibrary.org/conference-proceedings-of-spie/11597/115971E/Differentiation-of-Parkinsons-disease-and-non-Parkinsonian-olfactory-dysfunction-with/10.1117/12.2581233.short

57. Wierenga LM, Langen M, Oranje B, Durston S. Unique developmental trajectories of cortical thickness and surface area. Neuroimage. 2014 Feb 15;87:120–6.

58. Winkler AM, Kochunov P, Blangero J, Almasy L, Zilles K, Fox PT, et al. Cortical Thickness or Grey Matter Volume? The Importance of Selecting the Phenotype for Imaging Genetics Studies. Neuroimage. 2010 Nov 15;53(3):1135–46.

59. Panizzon MS, Fennema-Notestine C, Eyler LT, Jernigan TL, Prom-Wormley E, Neale M, et al. Distinct genetic influences on cortical surface area and cortical thickness. Cereb Cortex. 2009 Nov;19(11):2728–35.

60. Rahayel S, Bocti C, Sévigny Dupont P, Joannette M, Lavallée MM, Nikelski J, et al. Subcortical amyloid relates to cortical morphology in cognitively normal individuals. Eur J Nucl Med Mol Imaging. 2019 Oct;46(11):2358–69.

61. Sarasso E, Agosta F, Piramide N, Filippi M. Progression of grey and white matter brain damage in Parkinson's disease: a critical review of structural MRI literature. J Neurol [Internet]. 2020 May 6 [cited 2021 Jul 27]; Available from: https://doi.org/10.1007/s00415-020-09863-8

62. Donaghy PC, Firbank M, Petrides G, Lloyd J, Barnett N, Olsen K, et al. Diffusion imaging in dementia with Lewy bodies: Associations with amyloid burden, atrophy, vascular factors and clinical features. Parkinsonism & Related Disorders. 2020 Sep 1;78:109–15.

63. Unger MM, Belke M, Menzler K, Heverhagen JT, Keil B, Stiasny-Kolster K, et al. Diffusion tensor imaging in idiopathic REM sleep behavior disorder reveals microstructural changes in the brainstem, substantia nigra, olfactory region, and other brain regions. Sleep. 2010 Jun;33(6):767–73.

64. Scherfler C, Frauscher B, Schocke M, Iranzo A, Gschliesser V, Seppi K, et al. White and gray matter abnormalities in idiopathic rapid eye movement sleep behavior disorder: a diffusion-tensor imaging and voxel-based morphometry study. Ann Neurol. 2011 Feb;69(2):400–7.

65. Seubert J, Freiherr J, Frasnelli J, Hummel T, Lundström JN. Orbitofrontal Cortex and Olfactory Bulb Volume Predict Distinct Aspects of Olfactory Performance in Healthy Subjects. Cerebral Cortex. 2013 Oct 1;23(10):2448–56.

66. Frasnelli J, Lundström JN, Boyle JA, Djordjevic J, Zatorre RJ, Jones-Gotman M. Neuroanatomical correlates of olfactory performance. Exp Brain Res. 2010 Feb;201(1):1–11.

67. Rahayel S, Frasnelli J, Joubert S. The effect of Alzheimer's disease and Parkinson's disease on olfaction: a meta-analysis. Behav Brain Res. 2012 May 16;231(1):60–74.

68. Tremblay C, Mei J, Frasnelli J. Olfactory bulb surroundings can help to distinguish Parkinson's disease from non-parkinsonian olfactory dysfunction. NeuroImage: Clinical. 2020 Jan 1;28:102457.

69. Chepkoech J-L, Walhovd KB, Grydeland H, Fjell AM, Alzheimer's Disease Neuroimaging Initiative. Effects of change in FreeSurfer version on classification accuracy of patients with Alzheimer's disease and mild cognitive impairment. Hum Brain Mapp. 2016 May;37(5):1831–41.

Tables

Table 1. Demographic and clinical features in participants.

Variable	iRBD (A)	iRBD with MCI (B)	iRBD without MCI (C)	PD (D)	Controls (E)	p value, A vs. E	p value, A vs. D	p value, B vs. C
Age at MRI, years	65.8 (6.4)	67.9 (4.6)	64.8 (7.0)	64.8 (8.3)	63.2 (8.2)	0.09[b]	0.56[b]	0.080[b]
Men, n (%)	37 (77)	10 (63)	27 (84)	15 (50)	25 (61)	1.00[c]	0.014[c]	0.089[c]
Education, years	13.3 (3.7)	11.9 (3.8)	14.0 (3.4)	14.9 (3.8)	14.6 (4.1)	0.18[b]	0.061[b]	0.058[b]
RBD duration since symptom onset, years	12.1 (12.2)	13.3 (13.4)	11.5 (11.7)	-	-	-	-	0.47[d]
UPDRS-III, total score[a]	4.3 (3.6)	5.6 (5.0)	3.7 (2.6)	20.6 (9.2)	-	-	<0.001[d]	0.24[d]
MoCA, total score	25.7 (2.8)	24.1 (3.3)	26.9 (1.8)	-	-	-	-	0.005[d]

Values are presented as mean (SD).

PD: Parkinson's disease, iRBD: idiopathic rapid eye movement sleep behavior disorder, MCI: mild cognitive impairment, UPDRS-III: Unified Parkinson's Disease Rating Scale part III, MoCA: Montreal Cognitive Assessment.

[a]The UPDRS-III was measured in the 'on' state in PD patients.

[b]Student t test.

[c]Chi-squared test.

[d]Mann-Whitney U test.

Table 2. Results of the best performing models, brain regions and associated morphometric measurements used in the differentiation between participants.

Modality	Number of features	Recall	Precision	F1-score	Accuracy	Machine learning model	Brain region and characteristics in iRBD vs controls
Cortical thickness	1	0.640 (0.173)	0.702 (0.182)	0.661 (0.153)	0.640 (0.155)	Linear SVM, C = 1	thinning of paracentral lobule in iRBD (lh)
	5	0.712 (0.183)	0.725 (0.166)	0.710 (0.160)	0.684 (0.159)	Linear SVM, C = 1	thinning of paracentral lobule in iRBD (lh) thinning of medial orbital frontal cortex in iRBD (lh) thicker banks of the superior temporal sulcus in iRBD (lh) thinning of temporal pole in iRBD (lh) thinning of frontal pole in iRBD (rh)
Surface area	1	0.920 (0.183)	0.573 (0.069)	0.703 (0.108)	0.582 (0.108)	Linear SVM, C = 1	larger surface area of isthmus of cingulate cortex in iRBD (lh)
	5	0.800 (0.141)	0.721 (0.093)	0.754 (0.103)	0.716 (0.107)	Linear SVM, C = 1	larger surface area of isthmus of cingulate cortex in iRBD (lh) reduced surface area of rostral anterior cingulate cortex in iRBD (lh) larger surface area of precentral gyrus in iRBD (lh) reduced surface area of rostral middle frontal gyrus in iRBD (lh) larger surface area of temporal pole in iRBD (lh)
Volume	1	0.784 (0.152)	0.680 (0.150)	0.720 (0.124)	0.658 (0.157)	SVM with RBF kernel, C = 1	reduced volume of caudal middle frontal gyrus in iRBD (lh)
	5	0.832 (0.160)	0.735 (0.126)	0.775 (0.121)	0.733 (0.140)	SVM with RBF kernel, C = 1	reduced volume of caudal middle frontal gyrus in iRBD (lh) reduced volume of paracentral lobule in iRBD (lh) reduced volume of rostral anterior cingulate cortex in iRBD (lh) larger volume of fusiform gyrus in iRBD (rh) reduced volume of inferior parietal cortex in iRBD (rh)
Deformation	1	0.816 (0.140)	0.714 (0.113)	0.758 (0.112)	0.711 (0.132)	Linear SVM, C = 1	deformation of caudal middle frontal gyrus in iRBD (lh)
	5	0.768 (0.149)	0.852 (0.164)	0.803 (0.142)	0.791 (0.152)	Linear SVM, C = 1	deformation of caudal middle frontal gyrus in RBD (lh) deformation of paracentral lobule in iRBD (lh) deformation of thalamus proper in iRBD (lh) deformation of putamen in iRBD (lh) deformation of putamen in iRBD (rh)
All modalities	1	0.816 (0.140)	0.714 (0.113)	0.758 (0.112)	0.711 (0.132)	Linear SVM, C = 1	deformation of caudal middle frontal gyrus in iRBD (lh)
	5	0.776 (0.176)	0.855 (0.170)	0.806 (0.154)	0.796 (0.163)	Linear SVM, C = 1	deformation of caudal middle frontal gyrus in iRBD (lh) thinning of superior frontal gyrus in iRBD (lh) reduced volume of inferior parietal cortex in iRBD (rh) reduced volume of insula in iRBD (rh) deformation of putamen in iRBD (rh)

	Number of features	Recall	Precision	F1-score	Accuracy	Machine learning model	Brain region and characteristics in iRBD vs PD
All modalities	1	0.848 (0.145)	0.724 (0.073)	0.776 (0.086)	0.700 (0.102)	SVM with RBF kernel, C = 1	smaller volume of insula in iRBD (rh)
All modalities	2	0.880 (0.129)	0.786 (0.088)	0.828 (0.099)	0.775 (0.125)	SVM with RBF kernel, C = 1	smaller surface area of insula in iRBD (rh) lower thinning of entorhinal cortex in iRBD (rh)
All modalities	3	0.896 (0.131)	0.801 (0.114)	0.842 (0.105)	0.790 (0.134)	SVM with RBF kernel, C = 1	smaller surface area of insula in iRBD (rh) lower thinning of entorhinal cortex in iRBD (rh) lower thinning of lingual gyrus in iRBD (rh)
All modalities	5	0.904 (0.131)	0.832 (0.120)	0.863 (0.111)	0.820 (0.140)	SVM with RBF kernel, C = 1	smaller volume of insula in iRBD (rh) smaller surface area of insula in iRBD (rh) lower thinning of entorhinal cortex in iRBD (rh) lower thinning of lingual gyrus in iRBD (rh) greater volume of fusiform gyrus in iRBD (rh)
	Number of features	**Recall**	**Precision**	**F1-score**	**Accuracy**	**Machine learning model**	**Brain region and characteristics in iRBD with MCI vs without MCI**
All modalities	1	0.907 (0.205)	0.525 (0.094)	0.660 (0.127)	0.728 (0.079)	Decision tree, depth = 1	greater thinning of pars triangularis in iRBD with MCI (lh)
All modalities	2	0.907 (0.181)	0.537 (0.092)	0.667 (0.104)	0.732 (0.075)	Decision tree, depth = 1	greater thinning of pars triangularis in iRBD with MCI (lh) greater thinning of superior temporal gyrus in iRBD with MCI (lh)
All modalities	3	0.733 (0.236)	0.701 (0.188)	0.692 (0.160)	0.812 (0.093)	Linear SVM, C = 1	greater thinning of pars triangularis in iRBD with MCI (lh) greater thinning of transverse temporal cortex in iRBD with MCI (lh) deformation of isthmus of cingulate gyrus in iRBD with MCI (rh)
All modalities	5	0.787 (0.190)	0.749 (0.171)	0.754 (0.147)	0.848 (0.087)	Linear SVM, C = 1	greater thinning of pars triangularis in iRBD with MCI (lh) greater thinning of superior temporal gyrus in iRBD with MCI (lh) larger surface area of superior temporal gyrus in iRBD with MCI (lh) greater thinning of transverse temporal cortex in iRBD with MCI (lh) deformation of isthmus of cingulate gyrus in iRBD with MCI (rh)

Data are shown as mean (SD). All values reported are the average of model performance obtained from the test sets of the 25 randomly generated, unique train-test splits. iRBD: idiopathic rapid eye movement sleep behavior disorder, lh: left hemisphere, MCI: mild cognitive impairment, PD: Parkinson's disease, RBF: radial basis function, SVM: support vector machine, rh: right hemisphere.

Figures

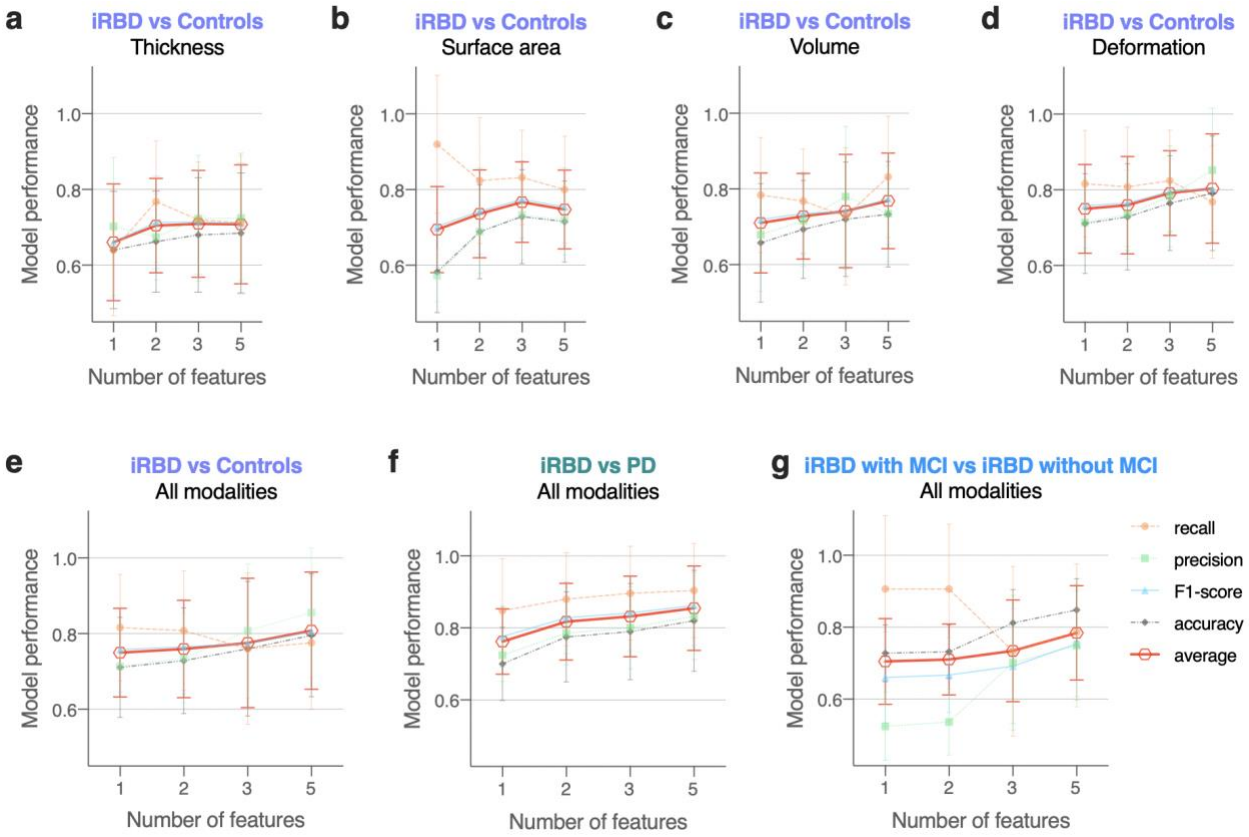

Figure 1. Results of machine learning models with the highest overall performance as measured by recall, precision, F1-score, accuracy, and average of the four metrics. (a-d) Outcomes of individual morphometric modalities in the differentiation between iRBD patients and controls. (e-g) Outcomes when all four morphometric modalities were merged and used in model training, for iRBD patients vs Controls (e), iRBD vs PD patients (f) and iRBD patients with MCI vs without MCI (g). iRBD: idiopathic rapid eye movement sleep behavior disorder, PD: Parkinson's disease, MCI: mild cognitive impairment. Error bars indicate standard deviation.

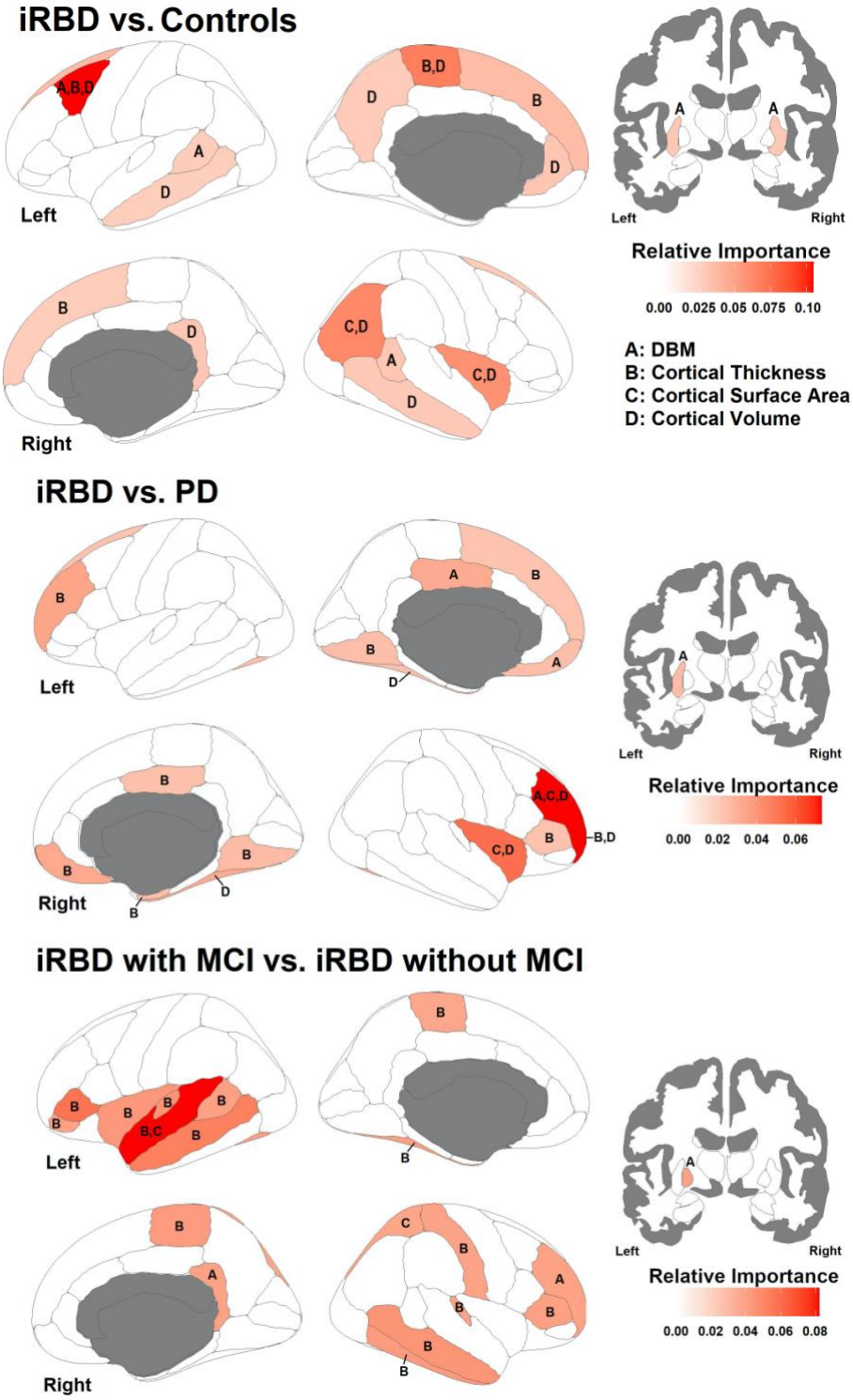

Figure 2. Relative importance of the top 20 most relevant brain regions in the discrimination between iRBD vs Controls (top), iRBD vs PD patients (middle) and iRBD patients with vs without MCI (bottom). The white-red color bar represents the relative importance of the feature in discriminating groups, with redder regions representing a more relevant feature. Every region from the top 20 is labeled from A-D in terms of the contributing structural metric (legend on the right). DBM: deformation-based morphometry, iRBD: idiopathic rapid eye movement sleep behavior disorder, MCI: mild cognitive impairment, PD: Parkinson's disease.

Supplementary materials

Supplementary Table 1. Morphometric measurements that differed significantly between controls and iRBD patients.

Morphometric modality and hemisphere	Brain region	Controls	iRBD	P value
Thickness, left	Superior frontal gyrus	2.55 (0.08)	2.48 (0.11)	0.001
	Paracentral lobule	2.39 (0.1)	2.32 (0.13)	0.005
	Temporal pole	3.53 (0.25)	3.38 (0.22)	0.015
	Inferior temporal gyrus	2.65 (0.12)	2.59 (0.12)	0.017
	Lateral orbital frontal cortex	2.52 (0.08)	2.47 (0.11)	0.025
	Middle temporal gyrus	2.70 (0.1)	2.65 (0.11)	0.033
	Rostral middle frontal gyrus	2.27 (0.07)	2.23 (0.08)	0.034
	Caudal middle frontal gyrus	2.45 (0.09)	2.41 (0.1)	0.038
	Pars orbitalis	2.51 (0.14)	2.44 (0.16)	0.038
	Precentral gyrus	2.52 (0.09)	2.46 (0.13)	0.049
Thickness, right	Superior frontal gyrus	2.51 (0.08)	2.46 (0.10)	0.008
	Precentral gyrus	2.50 (0.10)	2.42 (0.13)	0.011
	Supramarginal gyrus	2.45 (0.08)	2.40 (0.11)	0.013
	Frontal pole	2.49 (0.18)	2.41 (0.19)	0.027
	Middle temporal gyrus	2.76 (0.11)	2.70 (0.11)	0.031
	Insula	2.83 (0.14)	2.77 (0.13)	0.034
	Inferior parietal cortex	2.39 (0.08)	2.35 (0.11)	0.045
	Inferior temporal gyrus	2.69 (0.10)	2.64 (0.11)	0.045
Surface area, left	Caudal middle frontal gyrus	0.0016 (0.0002)	0.0015 (0.0002)	0.033
Volume, left	Paracentral lobule	0.0024 (0.0003)	0.0023 (0.0003)	0.003
	Caudal middle frontal gyrus	0.0042 (0.0007)	0.0039 (0.0005)	0.007
	Precuneus cortex	0.0064 (0.0006)	0.0062 (0.0007)	0.018
	Rostral anterior cingulate cortex	0.0018 (0.0003)	0.0016 (0.0003)	0.025
	Rostral middle frontal gyrus	0.0099 (0.0011)	0.0094 (0.0010)	0.025
	Middle temporal gyrus	0.0072 (0.0010)	0.0068 (0.0008)	0.042
Volume, right	Middle temporal gyrus	0.0077 (0.0009)	0.0073 (0.0007)	0.008

	Inferior parietal cortex	0.0094 (0.0010)	0.0090 (0.0011)	0.028
	Superior frontal gyrus	0.0138 (0.0014)	0.0134 (0.0012)	0.036
	Insula	0.0049 (0.0006)	0.0047 (0.0003)	0.042
Deformation, left	Putamen	0.94 (0.05)	0.91 (0.05)	0.003
	Caudal middle frontal gyrus	1.05 (0.08)	1.01 (0.05)	0.008
	Pallidum	0.94 (0.05)	0.91 (0.05)	0.017
	Rostral middle frontal gyrus	1.04 (0.04)	1.02 (0.03)	0.045
	Middle temporal gyrus	1.02 (0.04)	1.00 (0.04)	0.048
Deformation, right	Putamen	0.94 (0.05)	0.91 (0.05)	0.001
	Banks of superior temporal sulcus	1.02 (0.07)	0.98 (0.08)	0.012
	Pallidum	0.94 (0.05)	0.91 (0.05)	0.035

iRBD: idiopathic rapid eye movement sleep behavior disorder. Surface area and volume values were normalized using the estimated total intracranial volume. Red: Thinning, reduced surface area or volume, or tissue deformation value.

Supplementary Table 2. Morphometric measurements of individual modalities and their relative importance in the discrimination between iRBD patients and controls.

Brain region	Relative importance, thickness	Relative importance, surface area	Relative importance, volume	Relative importance, DBM
left banks superior temporal sulcus	**0.022305505**	0.017026148	0.01551811	0.027276656
left caudal anterior-cingulate cortex	0.021917045	0.016603306	0.015310066	0.016725567
left caudal middle frontal gyrus	0.020054339	0.028708748	**0.037178787**	**0.038762824**
left cuneus cortex	0.019823904	0.017993788	0.016980122	0.018192683
left entorhinal cortex	0.016420102	0.018692779	0.016810872	0.016864922
left fusiform gyrus	0.015018665	0.017888389	0.016618694	0.01713665
left inferior parietal cortex	0.016102759	0.018184875	0.018481313	0.015521528
left inferior temporal gyrus	0.021800697	0.016497	0.016601961	0.017306056
left isthmus of cingulate cortex	0.015078233	**0.023239002**	0.016779203	0.01662388
left lateral occipital cortex	0.016487876	0.020532328	0.021397511	0.020906932
left lateral orbital frontal cortex	0.021333901	0.016102995	0.018616616	0.016021742
left lingual gyrus	0.018026675	0.016489782	0.017506923	0.014279324
left medial orbital frontal cortex	**0.023591497**	0.017004424	0.015437216	0.014254237
left middle temporal gyrus	0.01875776	0.026214408	0.026351726	0.019466899
left parahippocampal gyrus	0.014762096	0.019797389	0.017922097	0.016020243
left paracentral lobule	**0.029715315**	0.02530747	**0.037866339**	**0.022335004**
left pars opercularis	0.018767494	0.01937071	0.016633876	0.019318701
left pars orbitalis	0.019122242	0.01647103	0.021289666	0.015001414
left pars triangularis	0.019499831	0.020506787	0.014673328	0.015989735
left pericalcarine cortex	0.01509976	0.016820632	0.017760814	0.014877758
left postcentral gyrus	0.018715116	0.020531452	0.016793803	0.021228537
left posterior cingulate cortex	0.020426057	0.023479751	0.021864193	0.015351491
left precentral gyrus	0.020623432	**0.02060851**	0.016201497	0.014979573
left precuneus cortex	0.014303085	0.021871517	0.027624118	0.013554826
left rostral anterior cingulate cortex	0.014175331	**0.024245328**	**0.031123506**	0.015931237
left rostral middle frontal gyrus	0.016952597	**0.022390423**	0.021800279	0.023693571
left superior frontal gyrus	0.035989948	0.015135126	0.018435064	0.01342881
left superior parietal cortex	0.020336566	0.015685343	0.016868388	0.015658986
left superior temporal gyrus	0.022095215	0.018781994	0.019603551	0.020587017
left supramarginal gyrus	0.022327884	0.017290019	0.015025562	0.020256599
left frontal pole	0.017658657	0.017294904	0.018096584	0.015977051
left temporal pole	**0.022407564**	**0.021304819**	0.01932195	0.025816837
left transverse temporal cortex	0.016772262	0.02180519	0.020804408	0.017494879
left insula	0.015511023	0.020521458	0.017205429	0.019213839
right banks superior temporal sulcus	0.015055823	0.025057231	0.017330523	0.030676689
right caudal anterior-cingulate cortex	0.015282552	0.021579249	0.016936631	0.013978628

right caudal middle frontal gyrus	0.01820841	0.023111299	0.017530615	0.016577496
right cuneus cortex	0.016235165	0.016492954	0.016100043	0.017883522
right entorhinal cortex	0.019727779	0.016930856	0.017574395	0.015617666
right fusiform gyrus	0.021679534	0.018988182	**0.022601389**	0.020638206
right inferior parietal cortex	0.022725407	0.026378884	**0.03655183**	0.016140729
right inferior temporal gyrus	0.024207126	0.019481885	0.019464448	0.021010259
right isthmus of cingulate cortex	0.020937058	0.017228661	0.029785904	0.015409167
right lateral occipital cortex	0.018025119	0.018985295	0.014909891	0.019491502
right lateral orbital frontal cortex	0.017221264	0.018562944	0.01577829	0.019164018
right lingual gyrus	0.018055113	0.018475632	0.022116586	0.01644412
right medial orbital frontal cortex	0.021264633	0.016324542	0.015309788	0.017731828
right middle temporal gyrus	0.017957595	0.023029289	0.029524627	0.020911868
right parahippocampal gyrus	0.023105728	0.017321952	0.017126039	0.015367507
right paracentral lobule	0.016499938	0.017703142	0.018555414	0.015645346
right pars opercularis	0.015302695	0.017939473	0.021031901	0.018084282
right pars orbitalis	0.016868545	0.016727673	0.014670288	0.014099411
right pars triangularis	0.016711051	0.017039055	0.016175176	0.015904235
right pericalcarine cortex	0.016757075	0.022129089	0.016912721	0.019618336
right postcentral gyrus	0.026053099	0.017304465	0.019567556	0.01444928
right posterior cingulate cortex	0.018465862	0.017455858	0.017160714	0.016300289
right precentral gyrus	0.025359234	0.019209346	0.015873759	0.015074336
right precuneus cortex	0.022266626	0.015349175	0.016591654	0.015985898
right rostral anterior cingulate cortex	0.0151598	0.019186566	0.013570289	0.013822434
right rostral middle frontal gyrus	0.01706589	0.017919454	0.020198454	0.017588874
right superior frontal gyrus	0.027164167	0.021448795	0.021236983	0.017921514
right superior parietal cortex	0.02387054	0.016644783	0.016728671	0.015802386
right superior temporal gyrus	0.024214295	0.016057021	0.019047373	0.015705328
right supramarginal gyrus	0.023733331	0.019294768	0.015270525	0.014208969
right frontal pole	**0.025218785**	0.020662633	0.018210874	0.01658924
right temporal pole	0.020047589	0.018626866	0.017645414	0.017588487
right transverse temporal cortex	0.016036985	0.020289195	0.017300682	0.016989113
right insula	0.019216359	0.027057868	0.03144684	0.01657214
left thalamus	N/A	N/A	N/A	**0.020805303**
left caudate	N/A	N/A	N/A	0.015308882
left putamen	N/A	N/A	N/A	**0.029251391**
left pallidum	N/A	N/A	N/A	0.024586336
left accumbensarea	N/A	N/A	N/A	0.015438647
left hippocampus	N/A	N/A	N/A	0.014339353
left amygdala	N/A	N/A	N/A	0.018576879
right thalamus	N/A	N/A	N/A	0.014462345

right caudate	N/A	N/A	N/A	0.014384861
right putamen	N/A	N/A	N/A	**0.035018443**
right pallidum	N/A	N/A	N/A	0.021360997
right accumbensarea	N/A	N/A	N/A	0.01797545
right hippocampus	N/A	N/A	N/A	0.01326785
right amygdala	N/A	N/A	N/A	0.012812538
brainstem	N/A	N/A	N/A	0.015305732

Blue indicates higher relative importance and red indicates lower relative importance. The 5 selected regions of each morphometric modality for the detection of iRBD, and the corresponding brain regions, are highlighted in red. iRBD: idiopathic rapid eye movement sleep behavior disorder.

Supplementary Table 3. Morphometric measurements of all modalities and their relative importance in the three classification tasks.

Modality	Brain region	Relative importance in iRBD vs controls	Relative importance in iRBD vs PD	Relative importance in iRBD with MCI vs without MCI
Thickness	left banks superior temporal sulcus	0.014079179	0.019549711	0.039856179
Thickness	left caudal anterior-cingulate cortex	0.013323188	0.017439446	0.030950973
Thickness	left caudal middle frontal gyrus	0.015908295	0.014067108	0.032876387
Thickness	left cuneus cortex	0.012438472	0.020779845	0.027326406
Thickness	left entorhinal cortex	0.011722899	0.020844082	0.030215824
Thickness	left fusiform gyrus	0.011117685	0.021353284	0.040265091
Thickness	left inferior parietal cortex	0.011371211	0.019143772	0.027155903
Thickness	left inferior temporal gyrus	0.017070415	0.014363645	0.031567695
Thickness	left isthmus of cingulate cortex	0.011348432	0.014659224	0.036294859
Thickness	left lateral occipital cortex	0.012300894	0.013603443	0.027268546
Thickness	left lateral orbital frontal cortex	0.016928141	0.019995745	0.030193138
Thickness	left lingual gyrus	0.011940763	0.024650088	0.023914679
Thickness	left medial orbital frontal cortex	0.017097566	0.015780046	0.022602326
Thickness	left middle temporal gyrus	0.015410157	0.014894575	0.052712822
Thickness	left parahippocampal gyrus	0.011322868	0.013668491	0.026288787
Thickness	left paracentral lobule	0.020753132	0.013227169	0.037548988
Thickness	left pars opercularis	0.015387613	0.018745183	0.031698277
Thickness	left pars orbitalis	0.015690116	0.021436755	0.039461592
Thickness	**left pars triangularis**	0.015793965	0.013653322	**0.056895199**
Thickness	left pericalcarine cortex	0.010990394	0.014033361	0.021892541
Thickness	left postcentral gyrus	0.012979236	0.015893163	0.036431948
Thickness	left posterior cingulate cortex	0.013707549	0.017613172	0.022848548
Thickness	left precentral gyrus	0.015142655	0.012640453	0.031494912
Thickness	left precuneus cortex	0.011822649	0.013012484	0.030116075
Thickness	left rostral anterior cingulate cortex	0.011416324	0.016209826	0.033126907
Thickness	left rostral middle frontal gyrus	0.014749473	0.034015919	0.024428467
Thickness	**left superior frontal gyrus**	**0.025514954**	0.022849732	0.035726972
Thickness	left superior parietal cortex	0.014691874	0.013201828	0.03084317
Thickness	**left superior temporal gyrus**	0.017493471	0.018006544	**0.043440949**
Thickness	left supramarginal gyrus	0.015530589	0.015291581	0.030474569
Thickness	left frontal pole	0.012287079	0.016768059	0.032179412
Thickness	left temporal pole	0.017097452	0.021108641	0.025326965
Thickness	**left transverse temporal cortex**	0.011206907	0.016753939	**0.044647084**
Thickness	left insula	0.012066725	0.014303357	0.043471837
Thickness	right banks superior temporal sulcus	0.011735428	0.014717026	0.033580899
Thickness	right caudal anterior-cingulate cortex	0.012268814	0.017172073	0.026779746
Thickness	right caudal middle frontal gyrus	0.014002181	0.013954758	0.027208521
Thickness	right cuneus cortex	0.012509784	0.014249984	0.035848189

Thickness	**right entorhinal cortex**	0.013100886	**0.023520966**	0.028327844
Thickness	right fusiform gyrus	0.013564742	0.022477871	0.023139147
Thickness	right inferior parietal cortex	0.017054597	0.014196839	0.024699917
Thickness	right inferior temporal gyrus	0.018581649	0.015156914	0.04246015
Thickness	right isthmus of cingulate cortex	0.016132018	0.016527631	0.024565563
Thickness	right lateral occipital cortex	0.012407566	0.013661633	0.034691799
Thickness	right lateral orbital frontal cortex	0.011851284	0.02041409	0.022329636
Thickness	**right lingual gyrus**	0.014716984	**0.026008193**	0.023324283
Thickness	right medial orbital frontal cortex	0.015246822	0.032514829	0.021846683
Thickness	right middle temporal gyrus	0.014854105	0.018723	0.044885561
Thickness	right parahippocampal gyrus	0.017089722	0.014476989	0.027128665
Thickness	right paracentral lobule	0.012402912	0.014473022	0.042459882
Thickness	right pars opercularis	0.01337562	0.016224865	0.021944947
Thickness	right pars orbitalis	0.012329492	0.017064422	0.032894184
Thickness	right pars triangularis	0.01167223	0.023241623	0.040046996
Thickness	right pericalcarine cortex	0.01253267	0.017935254	0.028649658
Thickness	right postcentral gyrus	0.016905022	0.012458152	0.039057056
Thickness	right posterior cingulate cortex	0.014214478	0.023800418	0.023898822
Thickness	right precentral gyrus	0.01877325	0.013969073	0.033584866
Thickness	right precuneus cortex	0.016414814	0.013399446	0.02763449
Thickness	right rostral anterior cingulate cortex	0.011465599	0.013708028	0.031977432
Thickness	right rostral middle frontal gyrus	0.013567612	0.021111272	0.024116962
Thickness	right superior frontal gyrus	0.021262416	0.016994278	0.024228412
Thickness	right superior parietal cortex	0.016248348	0.014227648	0.030410239
Thickness	right superior temporal gyrus	0.01645094	0.015434882	0.034222454
Thickness	right supramarginal gyrus	0.018551794	0.017093096	0.02892838
Thickness	right frontal pole	0.018494782	0.024654214	0.035391347
Thickness	right temporal pole	0.014120754	0.01574443	0.028458481
Thickness	right transverse temporal cortex	0.011560923	0.018638003	0.038637662
Thickness	right insula	0.015555332	0.022126482	0.024140652
Surface area	left banks superior temporal sulcus	0.011804736	0.014179616	0.028269495
Surface area	left caudal anterior-cingulate cortex	0.01185018	0.01859055	0.029566776
Surface area	left caudal middle frontal gyrus	0.018512643	0.013035388	0.03350493
Surface area	left cuneus cortex	0.012769615	0.013405796	0.027502303
Surface area	left entorhinal cortex	0.012240109	0.013116294	0.023918715
Surface area	left fusiform gyrus	0.011909125	0.02103983	0.035551085
Surface area	left inferior parietal cortex	0.013189596	0.013833195	0.023196357
Surface area	left inferior temporal gyrus	0.011866603	0.016749538	0.025251852
Surface area	left isthmus of cingulate cortex	0.015958487	0.0212881	0.025904815
Surface area	left lateral occipital cortex	0.013954291	0.014115729	0.020282852

Surface area	left lateral orbital frontal cortex	0.011776968	0.014264613	0.026393873
Surface area	left lingual gyrus	0.011346989	0.016227995	0.025677163
Surface area	left medial orbital frontal cortex	0.012088102	0.012660718	0.022317944
Surface area	left middle temporal gyrus	0.016399823	0.015984513	0.023282792
Surface area	left parahippocampal gyrus	0.013368721	0.01504468	0.026338249
Surface area	left paracentral lobule	0.01699631	0.019962389	0.033569856
Surface area	left pars opercularis	0.01306759	0.015761246	0.025735661
Surface area	left pars orbitalis	0.011664572	0.013192873	0.029988303
Surface area	left pars triangularis	0.014325188	0.019404746	0.029884263
Surface area	left pericalcarine cortex	0.011597313	0.013488359	0.031033441
Surface area	left postcentral gyrus	0.013699635	0.015344947	0.024285691
Surface area	left posterior cingulate cortex	0.015272823	0.013019238	0.025061639
Surface area	left precentral gyrus	0.01457001	0.017495095	0.026014717
Surface area	left precuneus cortex	0.014872035	0.02078623	0.031523674
Surface area	left rostral anterior cingulate cortex	0.015888193	0.014293146	0.024590174
Surface area	left rostral middle frontal gyrus	0.015299064	0.015526055	0.021310915
Surface area	left superior frontal gyrus	0.010837738	0.016967898	0.023230501
Surface area	left superior parietal cortex	0.011009514	0.014980647	0.025358578
Surface area	**left superior temporal gyrus**	0.012902697	0.015671332	**0.0389589**
Surface area	left supramarginal gyrus	0.011926347	0.017335015	0.020631152
Surface area	left frontal pole	0.012654333	0.015951619	0.023122464
Surface area	left temporal pole	0.01444723	0.01549076	0.028519145
Surface area	left transverse temporal cortex	0.014312613	0.017301175	0.029737349
Surface area	left insula	0.013577311	0.014702295	0.031563462
Surface area	right banks superior temporal sulcus	0.016863066	0.014034919	0.033839343
Surface area	right caudal anterior-cingulate cortex	0.015152306	0.013328578	0.027242533
Surface area	right caudal middle frontal gyrus	0.013912254	0.01455872	0.022370967
Surface area	right cuneus cortex	0.012085357	0.01442942	0.027223683
Surface area	right entorhinal cortex	0.011726925	0.012861287	0.031402504
Surface area	right fusiform gyrus	0.01278161	0.021168499	0.033555707
Surface area	right inferior parietal cortex	0.017478591	0.016535118	0.029827256
Surface area	right inferior temporal gyrus	0.014145474	0.020408667	0.027871193
Surface area	right isthmus of cingulate cortex	0.011884422	0.01784246	0.029194251
Surface area	right lateral occipital cortex	0.01306609	0.015053386	0.021983859
Surface area	right lateral orbital frontal cortex	0.013209152	0.012999835	0.024088024
Surface area	right lingual gyrus	0.012501777	0.014408485	0.029635258
Surface area	right medial orbital frontal cortex	0.011933068	0.016890827	0.021076271
Surface area	right middle temporal gyrus	0.015467286	0.015510372	0.027075188
Surface area	right parahippocampal gyrus	0.012023279	0.017357431	0.027573668
Surface area	right paracentral lobule	0.012697262	0.013617372	0.0319222

Surface area	right pars opercularis	0.01212243	0.018843115	0.023587593
Surface area	right pars orbitalis	0.011539456	0.01516969	0.02398069
Surface area	right pars triangularis	0.012133721	0.013781044	0.028122856
Surface area	right pericalcarine cortex	0.013336264	0.013580531	0.023448461
Surface area	right postcentral gyrus	0.012220051	0.013761146	0.022407599
Surface area	right posterior cingulate cortex	0.01260807	0.013966887	0.028512021
Surface area	right precentral gyrus	0.012877169	0.015832302	0.027681478
Surface area	right precuneus cortex	0.011143898	0.013881345	0.035642193
Surface area	right rostral anterior cingulate cortex	0.013272521	0.015343536	0.023819673
Surface area	right rostral middle frontal gyrus	0.012167336	0.024348844	0.037412131
Surface area	right superior frontal gyrus	0.014237726	0.013254355	0.021973606
Surface area	right superior parietal cortex	0.011395526	0.014338586	0.037711232
Surface area	right superior temporal gyrus	0.011665648	0.021516198	0.023668534
Surface area	right supramarginal gyrus	0.013394192	0.013299528	0.027350884
Surface area	right frontal pole	0.014360818	0.017266401	0.029843217
Surface area	right temporal pole	0.01334236	0.013353976	0.023126946
Surface area	right transverse temporal cortex	0.01336309	0.014229008	0.023982466
Surface area	**right insula**	0.016258779	**0.025296632**	0.02487458
Volume	left banks superior temporal sulcus	0.01163617	0.014304678	0.023475361
Volume	left caudal anterior-cingulate cortex	0.010949134	0.014700795	0.036370093
Volume	left caudal middle frontal gyrus	0.024401998	0.014446482	0.031566332
Volume	left cuneus cortex	0.012598747	0.013295854	0.023791372
Volume	left entorhinal cortex	0.011697937	0.012764738	0.025155303
Volume	left fusiform gyrus	0.012193735	0.02355814	0.030813691
Volume	left inferior parietal cortex	0.013478203	0.013416898	0.023191798
Volume	left inferior temporal gyrus	0.012192352	0.018309871	0.025962536
Volume	left isthmus of cingulate cortex	0.011947355	0.017714636	0.025129355
Volume	left lateral occipital cortex	0.01522789	0.015730507	0.021918332
Volume	left lateral orbital frontal cortex	0.014266613	0.015229908	0.021579694
Volume	left lingual gyrus	0.01271458	0.019659521	0.025987493
Volume	left medial orbital frontal cortex	0.011034274	0.014329334	0.022748933
Volume	left middle temporal gyrus	0.017221981	0.016602778	0.020612203
Volume	left parahippocampal gyrus	0.012548249	0.014730191	0.025405655
Volume	left paracentral lobule	0.024778782	0.017121263	0.021159391
Volume	left pars opercularis	0.012187552	0.013854126	0.023171459
Volume	left pars orbitalis	0.015518436	0.020967369	0.020793319
Volume	left pars triangularis	0.011315228	0.018658424	0.025683489
Volume	left pericalcarine cortex	0.012920082	0.013049061	0.027496995
Volume	left postcentral gyrus	0.012876342	0.014906299	0.031058686
Volume	left posterior cingulate cortex	0.015052976	0.01418775	0.03070179

Volume	left precentral gyrus	0.013001932	0.01404499	0.022697306
Volume	left precuneus cortex	0.019891012	0.015616971	0.022750903
Volume	left rostral anterior cingulate cortex	0.020981126	0.018706983	0.022336571
Volume	left rostral middle frontal gyrus	0.015871038	0.018796474	0.023478204
Volume	left superior frontal gyrus	0.014434799	0.01724332	0.022974848
Volume	left superior parietal cortex	0.011783881	0.013500984	0.024786328
Volume	left superior temporal gyrus	0.015408704	0.015510599	0.026953967
Volume	left supramarginal gyrus	0.011522122	0.020662282	0.024785635
Volume	left frontal pole	0.013374742	0.014815862	0.027308285
Volume	left temporal pole	0.014150304	0.018647726	0.024455756
Volume	left transverse temporal cortex	0.01374447	0.018369561	0.028298155
Volume	left insula	0.01217071	0.01472274	0.0253114
Volume	right banks superior temporal sulcus	0.013073473	0.017001092	0.024171755
Volume	right caudal anterior-cingulate cortex	0.013246974	0.014727398	0.023812067
Volume	right caudal middle frontal gyrus	0.01208595	0.013710942	0.02330445
Volume	right cuneus cortex	0.011473418	0.013178819	0.022201736
Volume	right entorhinal cortex	0.012413295	0.015339423	0.037047848
Volume	**right fusiform gyrus**	0.015864219	**0.031892986**	0.036795807
Volume	**right inferior parietal cortex**	**0.024129616**	0.017402507	0.026931811
Volume	right inferior temporal gyrus	0.014520287	0.018309896	0.023086281
Volume	right isthmus of cingulate cortex	0.01921661	0.018458416	0.028386609
Volume	right lateral occipital cortex	0.011076955	0.018065395	0.024462789
Volume	right lateral orbital frontal cortex	0.012490477	0.01674574	0.022536365
Volume	right lingual gyrus	0.015044684	0.017413527	0.027544467
Volume	right medial orbital frontal cortex	0.011896461	0.012634484	0.021296098
Volume	right middle temporal gyrus	0.020168018	0.015632793	0.021764322
Volume	right parahippocampal gyrus	0.012209865	0.019874645	0.028151478
Volume	right paracentral lobule	0.013771375	0.016760677	0.023085602
Volume	right pars opercularis	0.013960044	0.020564297	0.028574734
Volume	right pars orbitalis	0.011454239	0.014614335	0.022464252
Volume	right pars triangularis	0.011098119	0.013723619	0.022957657
Volume	right pericalcarine cortex	0.012562483	0.01596943	0.023239643
Volume	right postcentral gyrus	0.014665665	0.013871988	0.027270573
Volume	right posterior cingulate cortex	0.011608123	0.012336501	0.024783097
Volume	right precentral gyrus	0.012587535	0.013019264	0.020992576
Volume	right precuneus cortex	0.011828327	0.015049186	0.027861762
Volume	right rostral anterior cingulate cortex	0.010981158	0.015875024	0.023987197
Volume	right rostral middle frontal gyrus	0.014935121	0.025707931	0.02941208
Volume	right superior frontal gyrus	0.016122175	0.0164729	0.024702794
Volume	right superior parietal cortex	0.012020065	0.014489253	0.023803039

Volume	right superior temporal gyrus	0.014277264	0.015745437	0.02359007
Volume	right supramarginal gyrus	0.011621179	0.012922611	0.021889786
Volume	right frontal pole	0.013687657	0.025410771	0.02934109
Volume	right temporal pole	0.012320566	0.014939848	0.023471438
Volume	right transverse temporal cortex	0.012489608	0.012981911	0.024938289
Volume	**right insula**	**0.021323892**	**0.027336652**	0.025125714
Deformation	left banks superior temporal sulcus	0.020139406	0.014448023	0.023410098
Deformation	left caudal anterior-cingulate cortex	0.012518083	0.014971862	0.023583531
Deformation	**left caudal middle frontal gyrus**	**0.026359012**	0.022439221	0.02198052
Deformation	left cuneus cortex	0.015035229	0.014231586	0.028490458
Deformation	left entorhinal cortex	0.01323186	0.01294874	0.027161767
Deformation	left fusiform gyrus	0.014534996	0.014234563	0.02199874
Deformation	left inferior parietal cortex	0.011808512	0.013867425	0.024679826
Deformation	left inferior temporal gyrus	0.014119562	0.016837995	0.02948465
Deformation	left isthmus of cingulate cortex	0.013517441	0.016947317	0.030175269
Deformation	left lateral occipital cortex	0.015955581	0.019697677	0.02135947
Deformation	left lateral orbital frontal cortex	0.012147063	0.016011764	0.022333903
Deformation	left lingual gyrus	0.011536185	0.017011561	0.022233982
Deformation	left medial orbital frontal cortex	0.011217434	0.024784672	0.025018164
Deformation	left middle temporal gyrus	0.016187467	0.014148576	0.028300535
Deformation	left parahippocampal gyrus	0.012369806	0.017078687	0.037010084
Deformation	left paracentral lobule	0.016176805	0.021102808	0.031619591
Deformation	left pars opercularis	0.014941853	0.013315829	0.022823418
Deformation	left pars orbitalis	0.011568726	0.015501357	0.029512368
Deformation	left pars triangularis	0.012192376	0.017883305	0.026281511
Deformation	left pericalcarine cortex	0.012191062	0.013144696	0.021064911
Deformation	left postcentral gyrus	0.017498254	0.012547789	0.026571902
Deformation	left posterior cingulate cortex	0.012396343	0.032003898	0.031165804
Deformation	left precentral gyrus	0.011497233	0.013397404	0.025165174
Deformation	left precuneus cortex	0.011212541	0.017388392	0.022359431
Deformation	left rostral anterior cingulate cortex	0.01279649	0.017073704	0.022159183
Deformation	left rostral middle frontal gyrus	0.017125414	0.01929352	0.035351476
Deformation	left superior frontal gyrus	0.010788915	0.016492326	0.028676281
Deformation	left superior parietal cortex	0.011943207	0.014287664	0.021282456
Deformation	left superior temporal gyrus	0.01602699	0.016573515	0.025785755
Deformation	left supramarginal gyrus	0.016132979	0.013050433	0.023144003
Deformation	left frontal pole	0.012682229	0.014324081	0.024920648
Deformation	left temporal pole	0.018384577	0.014301561	0.023326803
Deformation	left transverse temporal cortex	0.013562159	0.015069344	0.026169376
Deformation	left insula	0.014360485	0.016721512	0.035604736

Deformation	right banks superior temporal sulcus	0.02246122	0.0132415	0.026333088
Deformation	right caudal anterior-cingulate cortex	0.011695458	0.012276017	0.022584054
Deformation	right caudal middle frontal gyrus	0.01259305	0.019684074	0.024045628
Deformation	right cuneus cortex	0.014762746	0.01353393	0.024798605
Deformation	right entorhinal cortex	0.012181006	0.013245076	0.026334405
Deformation	right fusiform gyrus	0.015518617	0.014724211	0.026507709
Deformation	right inferior parietal cortex	0.012860464	0.018053868	0.022338962
Deformation	right inferior temporal gyrus	0.01733522	0.0133652	0.022688264
Deformation	**right isthmus of cingulate cortex**	0.01241632	0.016685857	**0.039285114**
Deformation	right lateral occipital cortex	0.014731728	0.013113821	0.027053321
Deformation	right lateral orbital frontal cortex	0.014701487	0.013380676	0.024966149
Deformation	right lingual gyrus	0.013118936	0.017885638	0.021338641
Deformation	right medial orbital frontal cortex	0.014793091	0.015301727	0.022287184
Deformation	right middle temporal gyrus	0.017034367	0.014137359	0.025590129
Deformation	right parahippocampal gyrus	0.011936899	0.013551665	0.032585538
Deformation	right paracentral lobule	0.011903223	0.012701943	0.032846536
Deformation	right pars opercularis	0.013533817	0.013998113	0.032443056
Deformation	right pars orbitalis	0.011231039	0.02009125	0.028041412
Deformation	right pars triangularis	0.012333417	0.01750689	0.023309404
Deformation	right pericalcarine cortex	0.015503081	0.0128513	0.023601159
Deformation	right postcentral gyrus	0.011489251	0.014301173	0.02341984
Deformation	right posterior cingulate cortex	0.012926597	0.017864468	0.023355027
Deformation	right precentral gyrus	0.011740956	0.015612647	0.02123393
Deformation	right precuneus cortex	0.012794881	0.016704011	0.023945819
Deformation	right rostral anterior cingulate cortex	0.010942776	0.012748099	0.023831637
Deformation	right rostral middle frontal gyrus	0.013931446	0.02327875	0.03940495
Deformation	right superior frontal gyrus	0.01376992	0.013001065	0.024142899
Deformation	right superior parietal cortex	0.012356985	0.020700551	0.022328288
Deformation	right superior temporal gyrus	0.012290483	0.015964187	0.028270222
Deformation	right supramarginal gyrus	0.010969915	0.013459052	0.022989722
Deformation	right frontal pole	0.012854473	0.014403872	0.030211319
Deformation	right temporal pole	0.014006673	0.016264848	0.022342454
Deformation	right transverse temporal cortex	0.012921095	0.013714227	0.030880462
Deformation	right insula	0.013508908	0.015752182	0.024881475
Deformation	left thalamus	0.016088914	0.014288133	0.025419124
Deformation	left caudate	0.012198555	0.012931672	0.025281209
Deformation	left putamen	0.021505507	0.025581131	0.033742741
Deformation	left pallidum	0.018876772	0.020081253	0.039167822
Deformation	left accumbens area	0.012475014	0.0192723	0.025813701
Deformation	left hippocampus	0.011783754	0.014219076	0.02916447

Deformation	left amygdala	0.015219171	0.012917429	0.030234155
Deformation	right thalamus	0.011626025	0.015914864	0.028790682
Deformation	right caudate	0.011884908	0.01183014	0.024841387
Deformation	**right putamen**	**0.024620056**	0.019946589	0.034625928
Deformation	right pallidum	0.016529018	0.014116426	0.034465437
Deformation	right accumbens area	0.014147189	0.015978305	0.027909382
Deformation	right hippocampus	0.011570919	0.013928616	0.030238036
Deformation	right amygdala	0.010849397	0.014988168	0.027716113
Deformation	brainstem	0.011710106	0.013054873	0.023888922

Blue indicates higher relative importance and red indicates lower relative importance. The 5 selected regions in each classification, and the corresponding brain regions, are highlighted in red. iRBD: idiopathic rapid eye movement sleep behavior disorder. PD: Parkinson's disease. MCI: mild cognitive impairment.

Supplementary Table 4. Morphometric measurements that differed significantly between PD and iRBD patients.

Morphometric modality and hemisphere	Brain region	PD	iRBD	P value
Thickness, left	Lingual gyrus	1.95 (0.08)	2.00 (0.08)	0.003
	Rostral middle frontal gyrus	2.29 (0.09)	2.23 (0.08)	0.005
	Superior frontal gyrus	2.55 (0.08)	2.48 (0.11)	0.009
	Pars orbitalis	2.52 (0.14)	2.44 (0.16)	0.046
Thickness, right	Medial orbital frontal cortex	2.33 (0.14)	2.24 (0.10)	0.003
	Frontal pole	2.56 (0.25)	2.41 (0.19)	0.005
	Entorhinal cortex	2.99 (0.23)	3.13 (0.19)	0.013
	Pericalcarine cortex	1.72 (0.13)	1.79 (0.12)	0.028
	Posterior cingulate cortex	2.33 (0.15)	2.26 (0.11)	0.033
	Pars triangularis	2.30 (0.12)	2.26 (0.11)	0.040
	Lingual gyrus	1.98 (0.10)	2.02 (0.08)	0.043
Surface area, left	Isthmus of cingulate cortex	0.00071 (0.0001)	0.00075 (0.0001)	0.046
Volume, left	Fusiform gyrus	0.0057 (0.0005)	0.0060 (0.0006)	0.020
	Lingual gyrus	0.0040 (0.0006)	0.0043 (0.0006)	0.025
Volume, right	Fusiform gyrus	0.0057 (0.0005)	0.0062 (0.0009)	0.002
	Frontal pole	0.0007 (0.0001)	0.0007 (0.0001)	0.04992
Deformation, left	Posterior cingulate cortex	1.00 (0.06)	0.97 (0.05)	0.007
	Pallidum	0.93 (0.06)	0.91 (0.05)	0.039
	Accumbens area	1.01 (0.04)	0.99 (0.05)	0.049
	Putamen	0.93 (0.06)	0.91 (0.05)	0.04992

PD: Parkinson's disease, iRBD: idiopathic rapid eye movement sleep behavior disorder. Surface area and volume values were normalized using the estimated total intracranial volume. Red: Thinning, reduced surface area or volume, or tissue deformation value.

Supplementary Table 5. Morphometric measurements that differed significantly between iRBD patients with or without MCI.

Morphometric modality and hemisphere	Brain region	iRBD without MCI	iRBD with MCI	P value
Thickness, left	Pars triangularis	2.33 (0.11)	2.21 (0.06)	0.0002
	Pars orbitalis	2.49 (0.16)	2.35 (0.12)	0.005
	Superior temporal gyrus	2.64 (0.11)	2.53 (0.14)	0.006
	Transverse temporal cortex	2.35 (0.14)	2.23 (0.15)	0.006
	Middle temporal gyrus	2.68 (0.12)	2.60 (0.09)	0.007
	Insula	2.85 (0.13)	2.73 (0.13)	0.007
	Pars opercularis	2.45 (0.09)	2.38 (0.10)	0.022
	Banks of superior temporal sulcus	2.38 (0.08)	2.32 (0.10)	0.026
	Paracentral lobule	2.34 (0.13)	2.26 (0.12)	0.037
Thickness, right	Pars triangularis	2.29 (0.12)	2.19 (0.08)	0.007
	Middle temporal gyrus	2.73 (0.10)	2.65 (0.11)	0.010
	Paracentral lobule	2.39 (0.14)	2.32 (0.12)	0.010
	Postcentral gyrus	2.07 (0.12)	1.97 (0.12)	0.011
	Transverse temporal cortex	2.36 (0.14)	2.24 (0.18)	0.016
	Superior temporal gyrus	2.65 (0.13)	2.56 (0.14)	0.028
	Lateral occipital cortex	2.23 (0.09)	2.18 (0.08)	0.048
Surface area, left	Superior temporal gyrus	0.0026 (0.0002)	0.0028 (0.0002)	0.021
	Fusiform gyrus	0.0021 (0.0002)	0.0022 (0.0002)	0.031
	Paracentral lobule	0.0009 (0.0001)	0.0010 (0.0001)	0.041
Surface area, right	Precuneus cortex	0.0027 (0.0003)	0.0029 (0.0003)	0.031
	Paracentral lobule	0.0010 (0.0001)	0.0011 (0.0001)	0.048
Volume, right	Fusiform gyrus	0.0060 (0.0008)	0.0065 (0.0009)	0.025
Deformation, left	Pallidum	0.92 (0.05)	0.88 (0.05)	0.020
	Insula	1.00 (0.05)	1.04 (0.04)	0.031
Deformation, right	Isthmus of cingulate cortex	1.01 (0.06)	0.97 (0.05)	0.007
	Putamen	0.92 (0.05)	0.88 (0.04)	0.026
	Pallidum	0.92 (0.05)	0.89 (0.04)	0.033

iRBD: idiopathic rapid eye movement sleep behavior disorder. MCI: mild cognitive impairment. Surface area and volume values were normalized using the estimated total intracranial volume. Red: Thinning, reduced surface area or volume, or tissue deformation value.

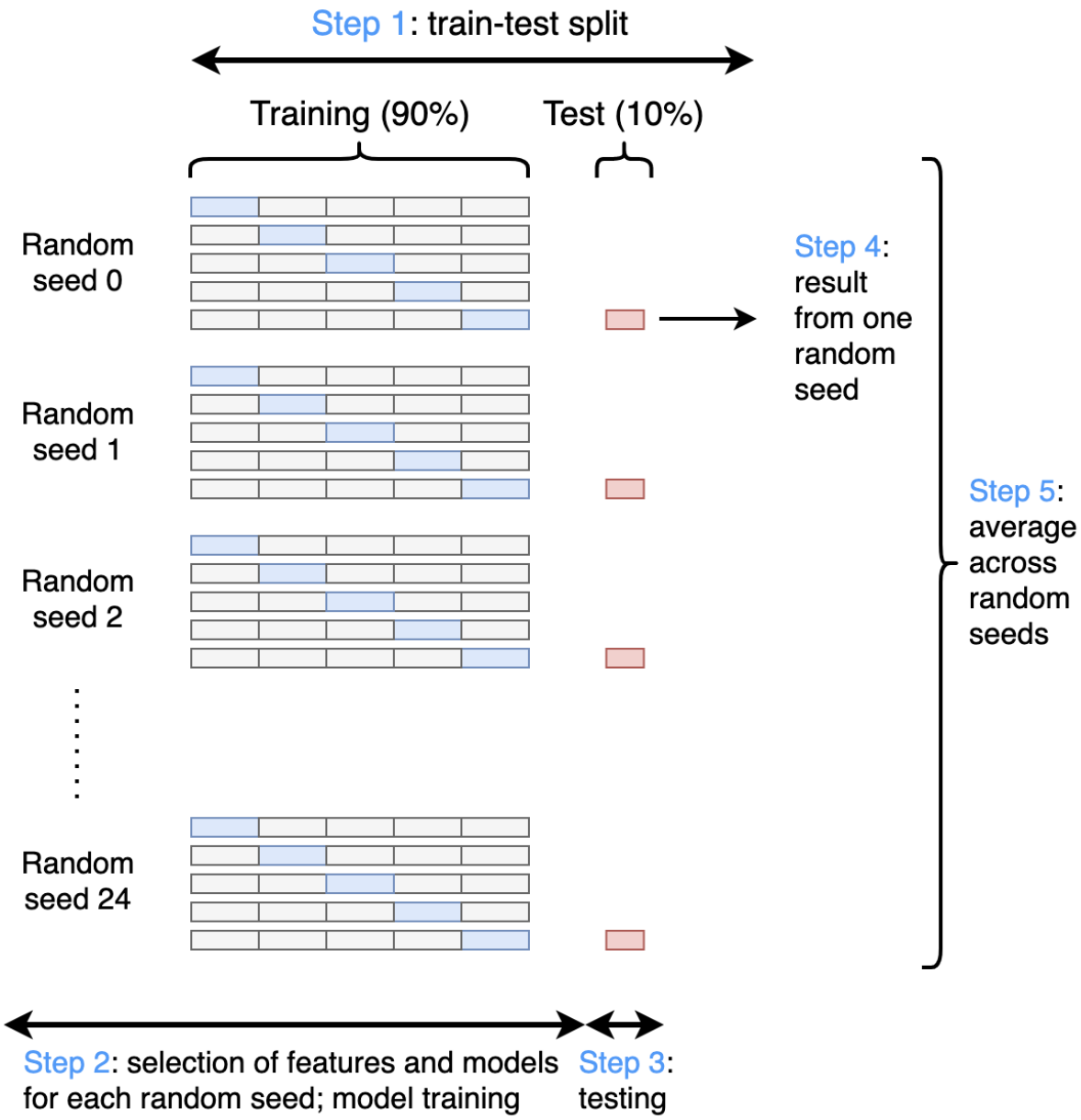

Supplementary Figure 1. A diagram demonstrating all steps of the proposed analysis, including random train-test split, feature and model selection, model training and testing, and evaluation of model performance.